


Lateral terminations of salt walls and megaflaps: An example from Gypsum Valley Diapir, Paradox Basin, Colorado, USA

Frederic O. Escosa¹  | Mark G. Rowan² | Katherine A. Giles³ | Kyle T. Deatrick³ | Allison M. Mast³ | Richard P. Langford³ | Thomas E. Hearon IV⁴ | Eduard Roca¹

¹Institut de Recerca Geomodels, Departament de Dinàmica de la Terra i de l'Oceà, Facultat de Ciències de la Terra, Universitat de Barcelona, Barcelona, Spain

²Rowan Consulting, Inc., Boulder, Colorado

³Institute of Tectonic Studies, Department of Geological Sciences, The University of Texas at El Paso, El Paso, Texas

⁴EOG Resources, Inc., Houston, Texas

Correspondence

Frederic O. Escosa, Institut de Recerca Geomodels, Departament de Dinàmica de la Terra i de l'Oceà, Facultat de Ciències de la Terra, Universitat de Barcelona, Barcelona, c/Martí i Franquès s/n, 08028, Spain.

Email: fredescosa@ub.edu

Funding information

Universitat de Barcelona, Grant/Award Number: SALTECRES (CGL2014-54118-C2-1-R); The University of Texas at El Paso; BHP; ExxonMobil; Hess; Kosmos; Repsol; BP; Chevron; ConocoPhillips; Shell

Abstract

Descriptions of exposed salt structures help improve the ability to interpret the geometry and evolution of similar structures imaged in seismic reflection data from salt-bearing sedimentary basins. This study uses detailed geologic mapping combined with well and seismic data from the southeastern end of the Gypsum Valley diapir (Paradox Basin, Colorado), to investigate the three-dimensional geometry of the terminations of both the salt wall and its associated megaflap. The salt wall trends NW-SE and is characterized by highly asymmetric stratal architecture on its northeastern and southwestern flanks, with thicker, deeper, gently dipping strata in the positionally proximal (NE) minibasin and thinned older strata rotated to near-vertical in a megaflap on the distal (SW) side. The megaflap terminates to the SE through a decrease in maximum dip and ultimately truncation by a pair of radial faults bounding a down-dropped block with lower dips. East of these faults, the salt wall termination is a moderately plunging nose of salt overlain by gently southeast-dipping strata, separated from the down-dropped NE minibasin by a counterregional fault. From this analysis, and by comparison with analogue structures located elsewhere in the Paradox Basin and in the northern Gulf of Mexico, we propose a series of simple end-member models in which salt walls and megaflaps may terminate abruptly or gradually. We suggest that controlling factors in determining these geometries include the original thickness and spatial distribution of the deep salt, the presence of nearby diapirs (which determines the fetch area for salt flow into the diapir), spatial patterns of depositional loading, and variations in the nature and location of salt breakout through the roof of the initial salt structure.

KEYWORDS

megaflaps, Paradox Basin, radial faults and counterregional faults, salt diapirs, salt walls

1 | INTRODUCTION

Steep-sided salt diapirs can have variable map-view shapes. They are termed salt stocks when the planform axial ratio

is <2 , and salt walls when it is >2 (Hudec & Jackson, 2011; Trusheim, 1960). Salt walls may form in a variety of tectonic settings. For example, they may result from extension (e.g. Zechstein Basin, Krzywiec, 2006; Mohr, Kukla,

This is an open access article under the terms of the Creative Commons Attribution License, which permits use, distribution and reproduction in any medium, provided the original work is properly cited.

© 2018 The Authors. *Basin Research* published by International Association of Sedimentologists and European Association of Geoscientists and Engineers and John Wiley & Sons Ltd

Urai, & Bresser, 2005; Atlas Mountains, Martín-Martín et al., 2016; Saura et al., 2013; Newfoundland, Balkwill & Legall, 1989). When the thick-skinned extension is decoupled by the presence of autochthonous salt, the walls typically develop above or slightly on the footwalls of the main presalt faults (Jackson & Vendeville, 1994). Conversely, salt walls may form during contraction (e.g. Sverdrup Basin, Harrison & Jackson, 2014; Sivas Basin, Kergaravat et al., 2016). For example, a salt-cored contractional anticline may be eroded, so that salt breaks through to form elongate diapirs (Stewart, 2007). Salt walls may also form by differential loading in the absence of extension or contraction (e.g. Paradox Basin, Trudgill, 2011; La Popa Basin, Rowan, Lawton, Giles, & Ratliff, 2003; Nordkapp Basin, Rowan & Lindsø, 2017), when progradational loading causes inflation above or immediately updip of the pre-existing presalt faults (Ge, Jackson, & Vendeville, 1997). In most cases, regardless of the triggering mechanism, they grow as passive diapirs once the salt has pierced its initial roof.

Stratal geometries flanking salt walls typically range from halokinetic sequences to megaflaps, depending on the scale of near-diapir deformation. Halokinetic sequences are localized (<1 km wide), unconformity-bound successions of growth strata that form as drape folds due to the interplay between the salt-rise rate and the sediment-accumulation rate (Giles & Lawton, 2002; Rowan et al., 2003). Stacked halokinetic sequences form tabular and tapered composite halokinetic sequences, which have relatively narrow and broad zones of thinning, respectively (Giles & Rowan, 2012). Megaflaps are panels of deep minibasin strata that extend far up the sides of steep diapirs or their equivalent welds (Giles & Rowan, 2012; Graham, Jackson, Pilcher, & Kilsdonk, 2012; Rowan, Giles, Hearon, & Fiduk, 2016). The width of folding and vertical relief of megaflaps span multiple kilometres, with the maximum bedding attitude ranging from near-vertical to completely overturned beneath an allochthonous salt sheet.

Many studies have focused on cross-sectional views of near-diapir deformation and thus are primarily two dimensional; three-dimensional analyses are relatively rare. Rowan, Lawton, and Giles (2012) showed along-strike variations in minibasin-scale folding, local halokinetic drape folding, and small-scale deformation of a welded salt wall in La Popa Basin. Similarly, Martín-Martín et al. (2016) determined the 3D geometry of the Tazoult salt wall in Morocco (including megaflaps), showing along-strike variations of flanking stratal geometries. In both cases the variations in stratal geometries were explained as being caused, in part by changes in the style and/or amount of shortening along the lengths of the walls. In contrast, Hearon, Rowan, Giles, and Hart (2014) tracked composite halokinetic sequences around the Auger salt

Highlights

- The Gypsum Valley salt wall is characterized by highly asymmetric stratal architecture on its NE and SW flanks.
- The SW flank comprises thinned, rotated strata in a megaflap that terminates to the SE by a decrease in dip and truncation by a radial fault.
- Strata on the NE flank are thicker, deeper, and only gently folded.
- The salt wall terminates to the SE in a moderately plunging nose of salt in the footwall of a NE-dipping counterregional fault.
- We propose end-member models in which salt walls and megaflaps may terminate abruptly or gradually.
- Controlling factors include the deep salt budget, the depositional loading pattern, and the position where the salts breaks through its early roof.

stock in the northern Gulf of Mexico, demonstrating that composite halokinetic sequences progressively change in geometry around the margin of the diapir and suggesting this was caused by local variations in diapir-roof thickness. Despite these studies, very little is known about strike-parallel changes in structural and stratigraphic architecture at the terminations of salt walls or megaflaps. Investigating this variability is important for a better understanding of salt-sediment interaction in three dimensions, as well as for aiding interpretations of poorly imaged seismic reflection data and thus risk assessment in hydrocarbon exploration.

The purpose of this paper is to present new data from the southeastern end of the Gypsum Valley salt wall, in the Paradox Basin of SW Colorado, in order to evaluate the structural styles and associated controls on lateral terminations of salt walls and megaflaps. The main goals are three-fold: (a) to build on the brief two-dimensional analysis of the Gypsum Valley megaflap in Rowan et al. (2016) and characterize the 3D structure and kinematic evolution of both the megaflap and southeastern end of the salt wall; (b) to compare our findings with other salt walls in the Paradox Basin, and analogous to counterregional systems in the northern Gulf of Mexico; and (c) to establish simple models for the lateral terminations of salt walls and megaflaps. We suggest that factors controlling the nature and geometry of these lateral terminations include the type and location of bounding structures, the salt budget for flow into the diapir, the spatial patterns of depositional loading, and variations in the style and location of salt breakout through the roof of the initial salt structure.

2 | GEOLOGICAL SETTING AND PREVIOUS WORK

2.1 | Paradox Basin

The Paradox Basin (SE Utah and SW Colorado, USA), is a large, asymmetric, intracratonic foreland basin defined by the depositional extent of the layered evaporites of the Pennsylvanian Paradox Formation (Figure 1a). The basin measures ca. 300 km in length (NW-SE) and ca. 150 km in width (Condon, 1997; Trudgill, 2011; Whidden, Lillis, Anna, Pearson, & Dubiel, 2013). During the Late

Mississippian to Early Permian time, convergent tectonism along the western margin of North America, coupled with the collision of Gondwanaland to the south, generated intraplate deformation in the form of a series of thick-skinned, basement-cored uplifts, extending from Canada to Mexico, known as the Ancestral Rocky Mountains (Barbeau, 2003; Kluth, 1986; Kluth & Coney, 1981; Mallory, 1972). Borehole and 2D seismic reflection data show the Paradox Basin (Figure 1a) is located in the footwall of a 50° NE-dipping reverse fault, with ca. 10 km of slip, bounding the southwestern flank of the basement-cored Uncompahgre Uplift (Moore, Soreghan, & Sweet, 2008;

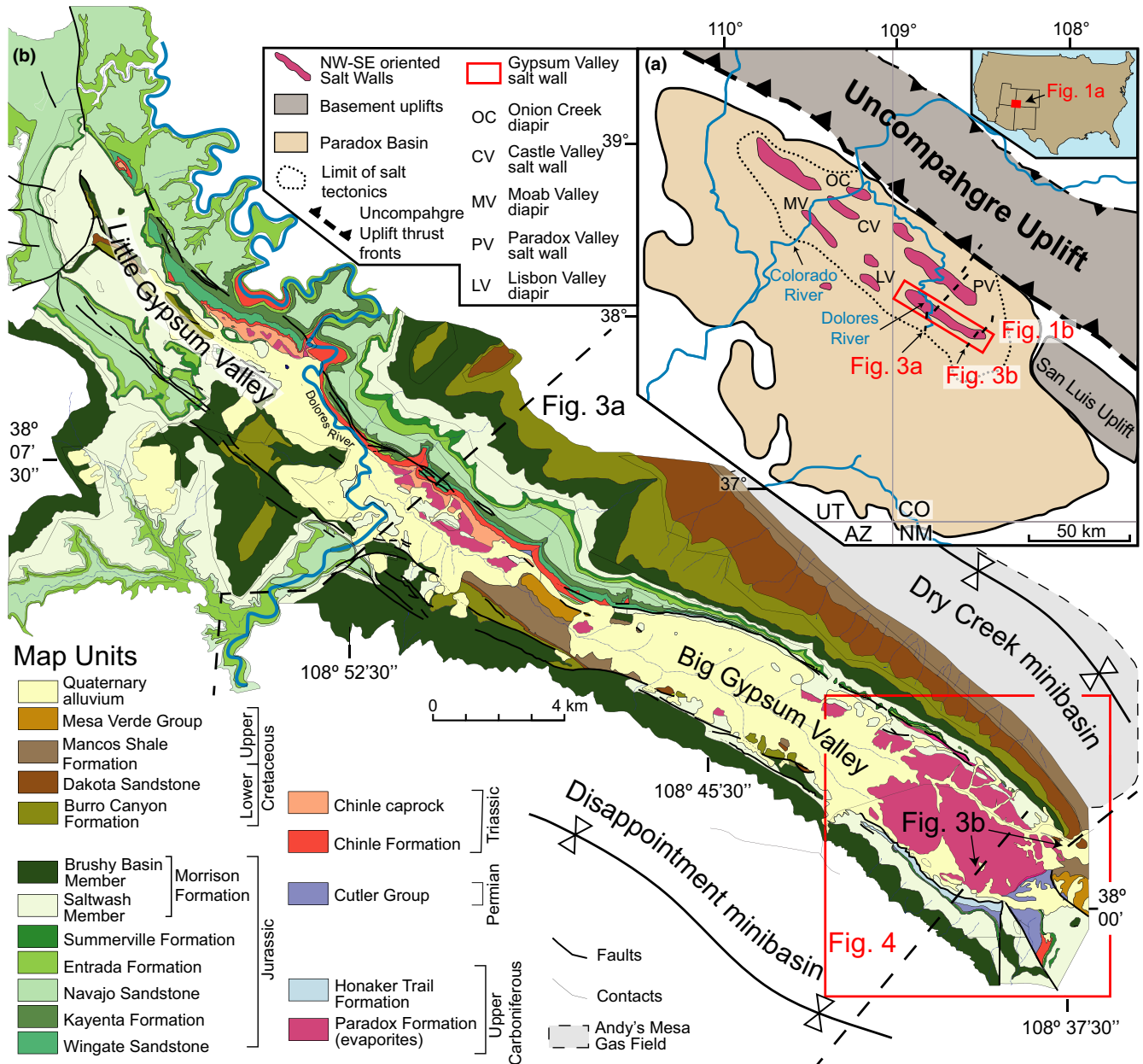


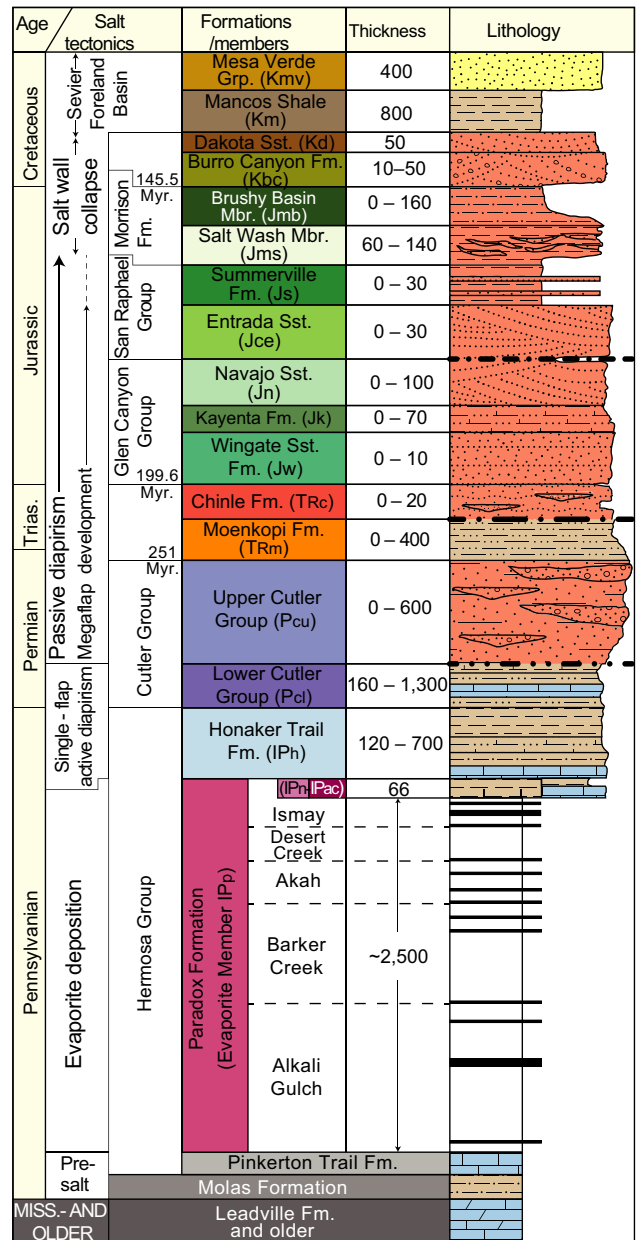
FIGURE 1 Location map: (a) Paradox Basin and its major salt walls (after Shoemaker, Case, & Elston, 1958); UT: Utah, CO: Colorado, AZ: Arizona, NM: New Mexico; (b) geologic map of Gypsum Valley salt wall. The red outlines indicate, in (a), the location of Fig. 1b, and in (b), the study area illustrated in Figure 4

Timbel, 2015; White & Jacobson, 1983). The emplacement of the Uncompahgre Uplift and concurrent flexural loading of the crust in its foreland created accommodation for sediment infill (Barbeau, 2003; Condon, 1997; DeCelles & Giles, 1996; Trudgill, 2011).

The Paradox Basin contains as much as ca. 7 km of Pennsylvanian to Cretaceous basin fill (Figure 2) adjacent to the Uncompahgre Uplift (Barbeau, 2003; Goldhammer, Oswald, & Dunn, 1994; Trudgill & Paz, 2009). The upper Paleozoic to Mesozoic section comprises four lithostratigraphic units separated by three regional unconformities (Figure 2). At the base is the Middle Pennsylvanian (Desmoinesian) Paradox Fm., a layered evaporite sequence that passes upward to mixed marine carbonates (Honaker Trail Fm.) and marine to nonmarine siliciclastics (lower Cutler Grp.). The mid-Cutler unconformity (which is readily imaged on seismic data; Figure 3a,b) separates this basal unit from those above, which comprise upper Cutler Grp. to Mesozoic alluvial, fluvial and eolian strata. These in turn are separated by two regional unconformities at the bases of the Chinle Fm. (Molenaar, 1981) and Entrada Sst. (Figure 2).

According to Barbeau (2003) and Blakey (2009), maximum subsidence of the Paradox Basin coincided with deposition of the Paradox Fm. evaporites. Subsequent differential loading by prograding Upper Pennsylvanian to Permian fluvial sediment, shed from the Uncompahgre Uplift (Figure 1a), caused salt inflation over presalt normal faults, thereby triggering a series of NW-SE trending salt walls (Baars & Stevenson, 1981; Elston, Shoemaker, & Landis, 1962; Ge et al., 1997; Kluth & DuChene, 2009; Lawton & Buck, 2006; Trudgill, 2011). The onset of diapirism was earlier in proximal (NE) than distal (SW) areas (Trudgill, 2011).

Throughout the basin, passive diapirism was a dominantly Permian event, with activity decreasing during the Triassic (Barbeau, 2003; Elston et al., 1962; Lawton & Buck, 2006; Trudgill, 2011). According to Rasmussen and Rasmussen (2009), diapirism across the deepest part of the basin ended in the Early Triassic. However, Vogel (1960) and later Rowan et al. (2016) interpret diapirism at Gypsum Valley, which is located in a distal position, to have ended by the mid-Jurassic. Importantly, although contraction was involved in the emplacement of the Uncompahgre Uplift, there is no cited evidence for any contraction in the Paradox Basin, except for minor shortening during the



* Thickness changes in the study area from minibasin to the top of the Gypsum Valley salt wall in meters (min-max)

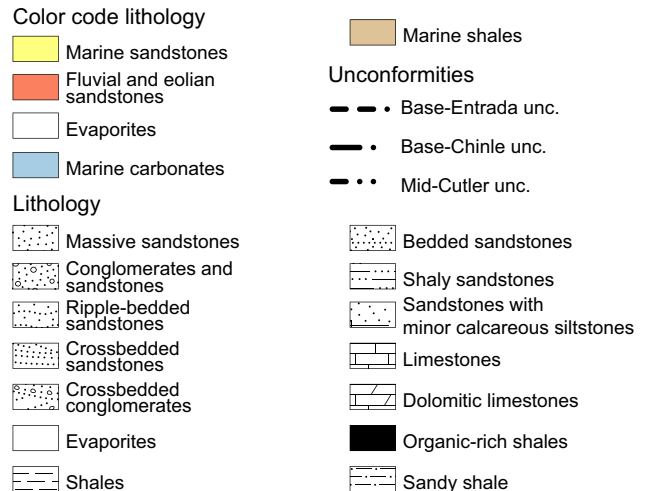


FIGURE 2 Stratigraphic column of the southern Paradox Basin including: the colours used in the geological map, cross sections and restoration; thickness variations; and simplified lithology with the three main unconformities (after Doelling, 2001; Trudgill, 2011). Salt tectonics phases are specific to the Gypsum Valley diapir and are not necessarily appropriate for other Paradox Basin salt walls

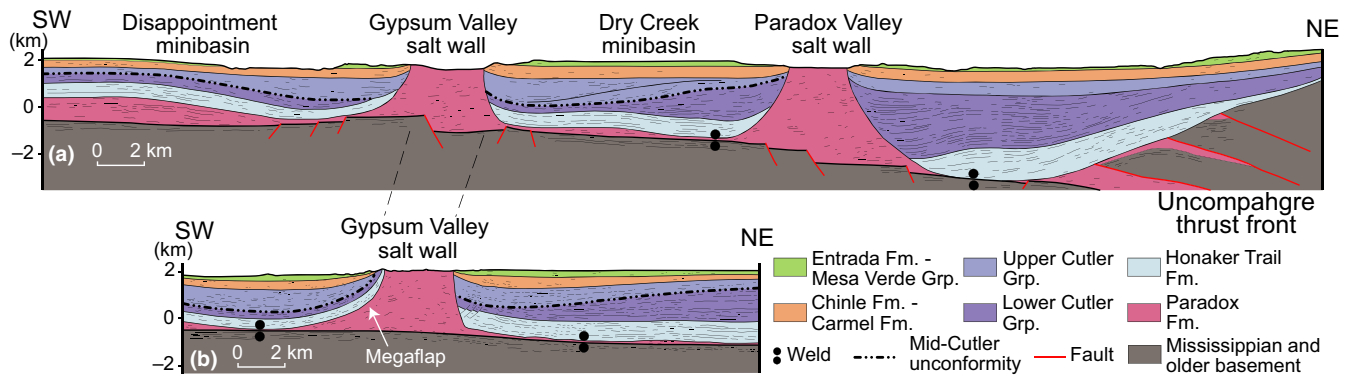


FIGURE 3 Line drawings of regional depth-converted seismic profiles in the southeastern Paradox Basin (see location in Figure 1): (a) across the centre of Gypsum Valley diapir and the southeastern end of the Paradox Valley diapir; (b) across the study area at the southeastern end of the Gypsum Valley salt wall modified from Rowan et al. (2016). Original data and depth conversions courtesy of ConocoPhillips

Laramide Orogeny, postdating salt wall formation and diapir burial (Mankowski, Campbell, Huntoon, Gregg, & Linari, 2002).

2.2 | Gypsum Valley salt wall

The Gypsum Valley diapir is a NW-SE trending vertical salt wall located in the southeastern, distal part of the Paradox Basin in SW Colorado (Figure 1). The salt wall is bounded on the northeastern side by the Dry Creek minibasin and on the southwestern side by the Disappointment minibasin, forming a breached anticline geometry almost 35 km long and from 2 to 3.5 km wide. The core of the structure has been eroded to form the Gypsum Valley physiographic feature, which is divided into a northern, narrower part referred to as Little Gypsum Valley, and a broader, southern part referred to as Big Gypsum Valley. The southeastern termination of the salt wall, at the southern end of the Big Gypsum Valley, is the focus of this study (Figures 1b and 4).

Seismic reflection, well, and field data depict an important asymmetry (Figure 3b) between the bounding minibasins of the study area (Amador, Schurger, & Miller, 2009; Rowan et al., 2016). On the northeastern side (Dry Creek minibasin), older (Upper Pennsylvanian to Permian) strata are relatively thick and deeply buried, with only minor upturn near the diapir. On a broad scale, Cutler Grp. strata form basinward (SW) shifting depocentres (Figure 3a,b) characteristic of expulsion–rollover structures (Ge et al., 1997; Trudgill, 2011). In contrast, the southwestern side (Disappointment minibasin, Figure 3b) is marked by Pennsylvanian strata that gradually becomes thin and upturns to the near-vertical adjacent to the diapir, forming a megaflap (Deatrick, Giles, Langford, Rowan, & Hearon, 2015; Mast, 2016; Rowan et al., 2016).

The general evolution of the southeastern part of this salt wall, based on a 2-D analysis and restoration (Rowan

et al., 2016), is depicted in Figure 5. Salt movement was triggered during the Late Pennsylvanian by differential sedimentary loading, forming an early, asymmetric, single-flap active diapir (Schultz-Ela, Jackson, & Vendeville, 1993) with a thinned roof bounded by a suprasalt counterregional fault over the proximal (NE) edge of the diapir (Figure 5b, c). Erosion of the thinned diapir roof (mid-Cutler unconformity) triggered salt breakthrough and the onset of passive diapirism (Figure 5d). Subsequent evacuation of deep salt into the growing diapir generated diapir-flanking depocentres containing upper Cutler Grp. and younger strata, with progressive rotation of the southwestern flank into the megaflap geometry and consequent widening of the diapir (Figure 5e,f).

3 | OBSERVATIONS

3.1 | Methods

To achieve the goals outlined for this study, both subsurface and field data were incorporated into the analysis. Subsurface data include one regional 2D depth-converted seismic reflection profile across the southeastern end of the Gypsum Valley salt wall (Figure 3b; Rowan et al., 2016). The interpretation in depth was constrained by horizon tops from 13 wells (see well locations in Figure 4). Field data include more than 1,200 stations with structural and stratigraphic data.

3.2 | Stratigraphy

According to field and well data (Baars, 1965; Hite & Buckner, 1981; Mahrer, Ake, O'Connell, & Block, 2012; Timbel, 2015; Weimer 1982), the nonoutcropping presalt units are Cambrian to lowermost Pennsylvanian carbonate and siliciclastic rocks (Figure 2). Overlying this, the thick Paradox Fm. contains 29 cycles of primarily halite,

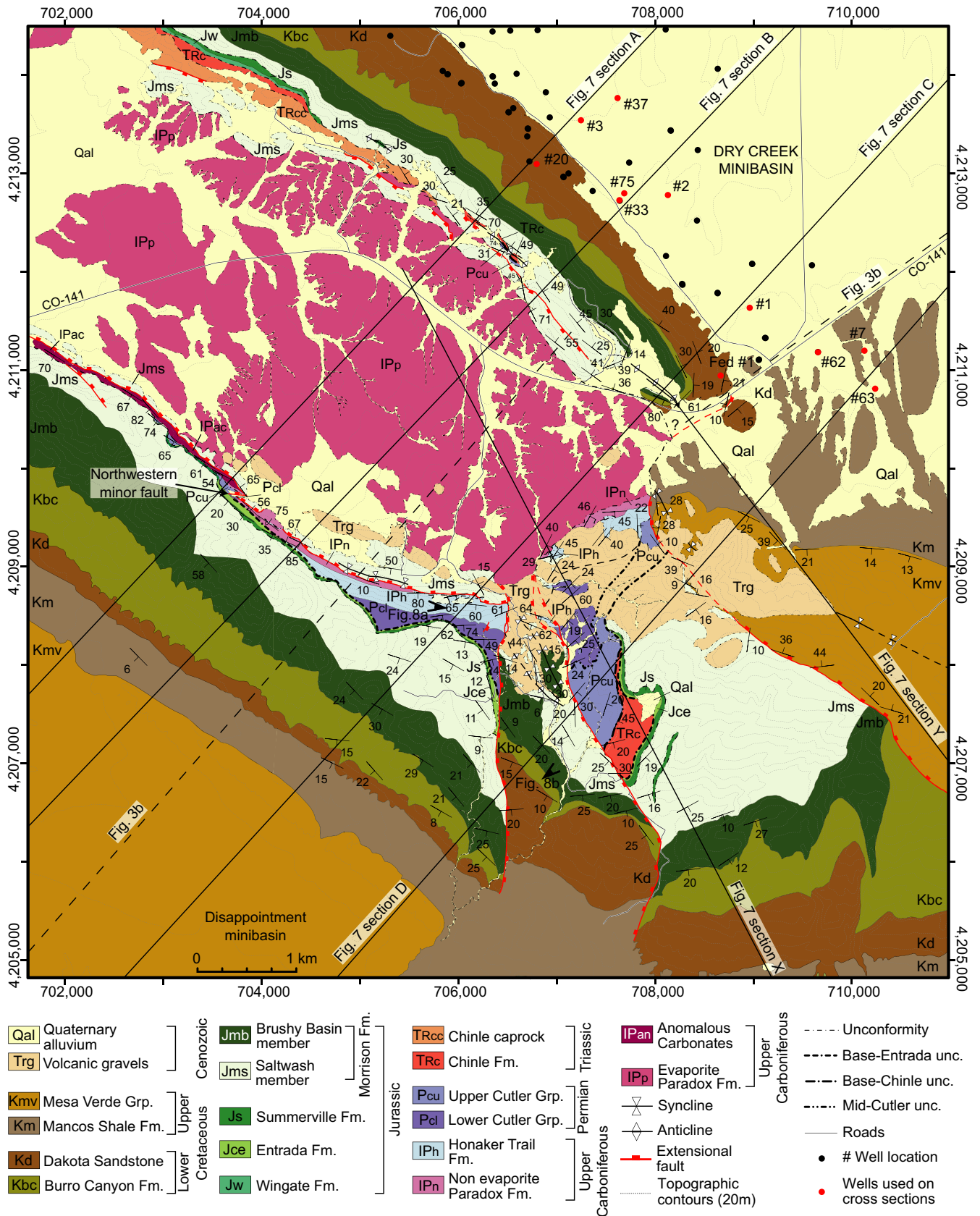


FIGURE 4 Detailed geologic map of the southeastern termination of the Gypsum Valley salt wall (location in Figure 1b), showing available well data, the trace of the cross sections (Figure 7), and the trace of the seismic profile shown in Figure 3b and restored in Figure 5. Stratigraphic colours and labels as in Figure 2. Coordinates are in metres in Universal Transverse Mercator, zone 12 northern hemisphere and datum NAD83

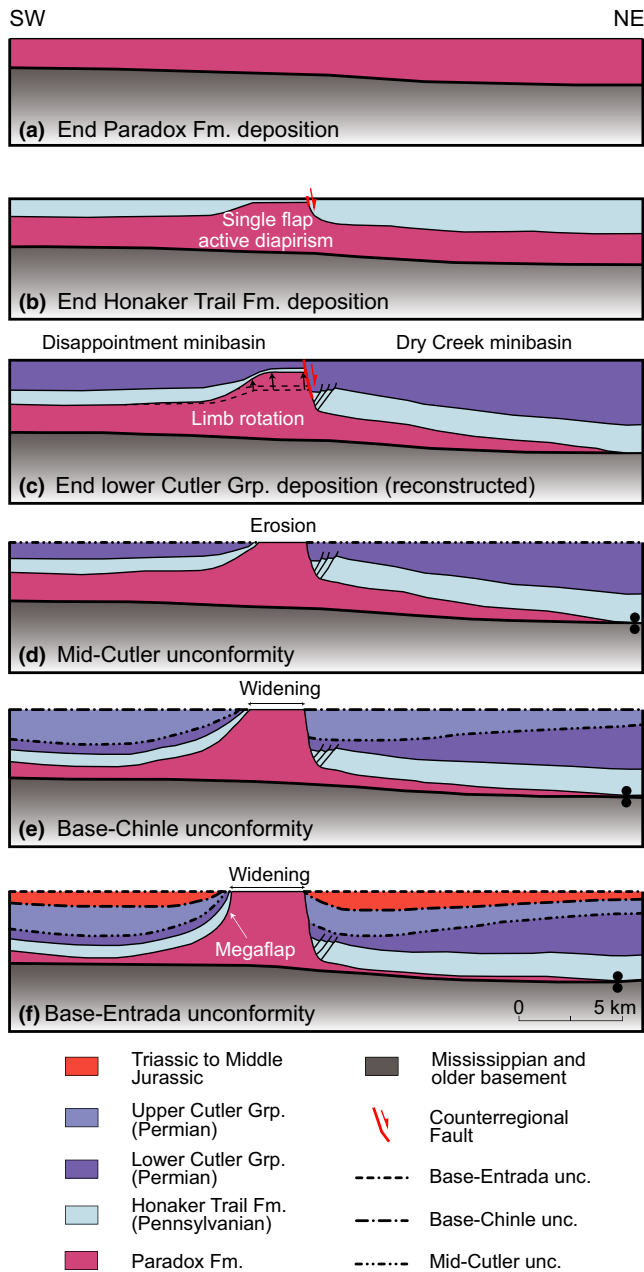


FIGURE 5 Sequential quantitative restoration of the Gypsum Valley salt wall (modified from Rowan et al., 2016) along the depth-converted seismic profile of Figure 3b

anhydrite, and organic mudstones (Figure 2) that are interbedded with coarse-grained siliciclastics in the fore-deep near the Uncompahgre Uplift and carbonates in the distal margins of the Paradox Basin, which includes Gypsum Valley (Franczyk, 1992; Goldhammer et al., 1994; Hite & Buckner, 1981; Lawton, Buller, & Parr, 2015; Nucio & Condon, 1996). The Paradox Fm. serves as the salt source for the Gypsum Valley diapir.

Stratal units influenced by concurrent salt tectonics range from the uppermost Ismay member, an informal rock unit of the Upper Pennsylvanian Paradox Fm., through the

Lower Cretaceous Dakota Sst. (Figure 2). On the southwestern flank of the diapir, the thinned package of the megaflap comprises: the uppermost Paradox Fm. shales and carbonates (Mast, 2016), the cyclic carbonate and siliciclastics of the Honaker Trail Fm., and the lower Cutler Grp. carbonates interbedded with shales (Deatrick et al., 2015). Growth strata recording passive diapirism are composed of the following: the upper Cutler Grp., the Moenkopi and Chinle formations, the Glen Canyon Grp. and the San Rafael Grp. (Figure 2). The lower Cutler fossiliferous carbonates and upper Cutler nonmarine red arkosic conglomerates and sandstones are separated by the mid-Cutler unconformity (Barbeau, 2003), and the base-Chinle unconformity divides marine fine-grained sediment of the Moenkopi Fm. from continental red sandstones and conglomerates of the Chinle Fm. (Doelling, 1988; Hazel, 1994; Molenaar, 1981; O'Sullivan & MacLachlan, 1975; Stewart, Poole, & Wilson, 1972). Above the base-Entrada unconformity, eolian and fluvial strata of the San Rafael Grp. (and younger units) have a different relationship to the diapir, overlapping the salt wall, thickening into synclines located over the top of the diapir in the Little Gypsum Valley, or exposed as blocks that have been faulted down onto the top of salt. Finally, the Mancos Shale and Mesa Verde Grp. (Figure 2) were deposited in the Sevier Foreland Basin (Lawton et al., 1997), by which time the salt wall was no longer active and was buried beneath at least a kilometre of sediment.

3.3 | Structural geometry

The southeastern end of the Gypsum Valley salt wall is subdivided into five structural domains (SD) that are bounded by different types of faults (Figure 6a). In the sections below, we describe first the faults and then the defining attributes of structural domains and sub-domains, generally moving from the megaflap counter-clockwise around the end of the diapir to the northeastern flank.

3.3.1 | Faults

Northwestern minor fault

A minor WNW-ESE trending fault on the SW flank of the Gypsum Valley salt wall divides structural domain I into two sub-domains, I' and I'' (Figure 6a). Although mostly covered by Quaternary sediment, the fault is inferred from the ca. 80 m offset of the Paradox-Cutler contact and associated different attitudes in strata on either side (Figure 4). Although the origin of the fault is unknown, the geometry is compatible with a down-to-the-N normal fault (Figure 7, section A inset). Moreover, it was active relatively early since it terminates at the base-Entrada unconformity (Figures 4 and 6a).

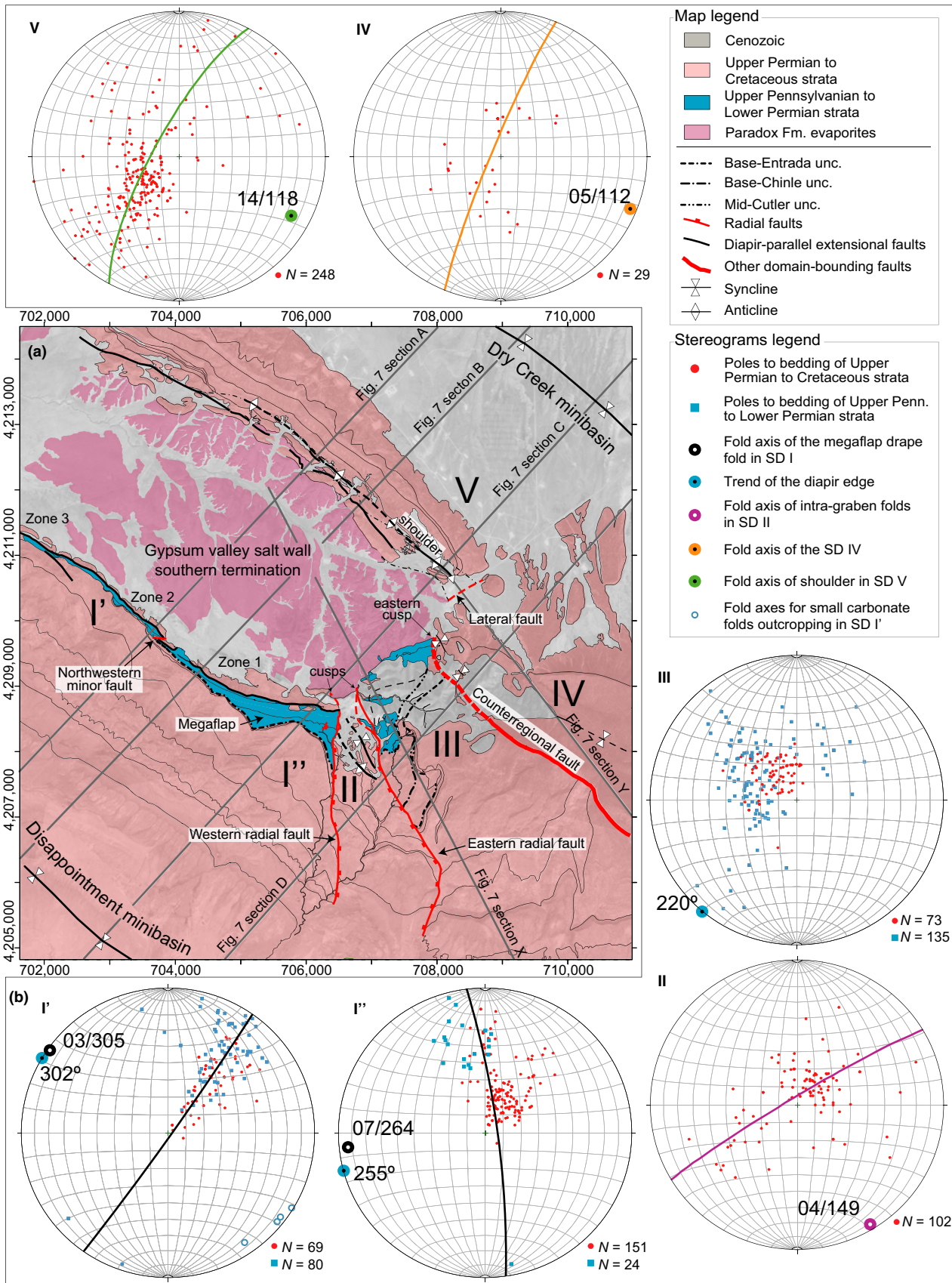


FIGURE 6 Structural domains: (a) black and white orthophoto overlain by the structural map of the study area and showing the division of the study area into five structural domains (Roman numerals); (b) lower-hemisphere equal-area (Schmidt) stereographic projections of structural data for each domain. Zones 1–3 along megaflap are those of Mast (2016)

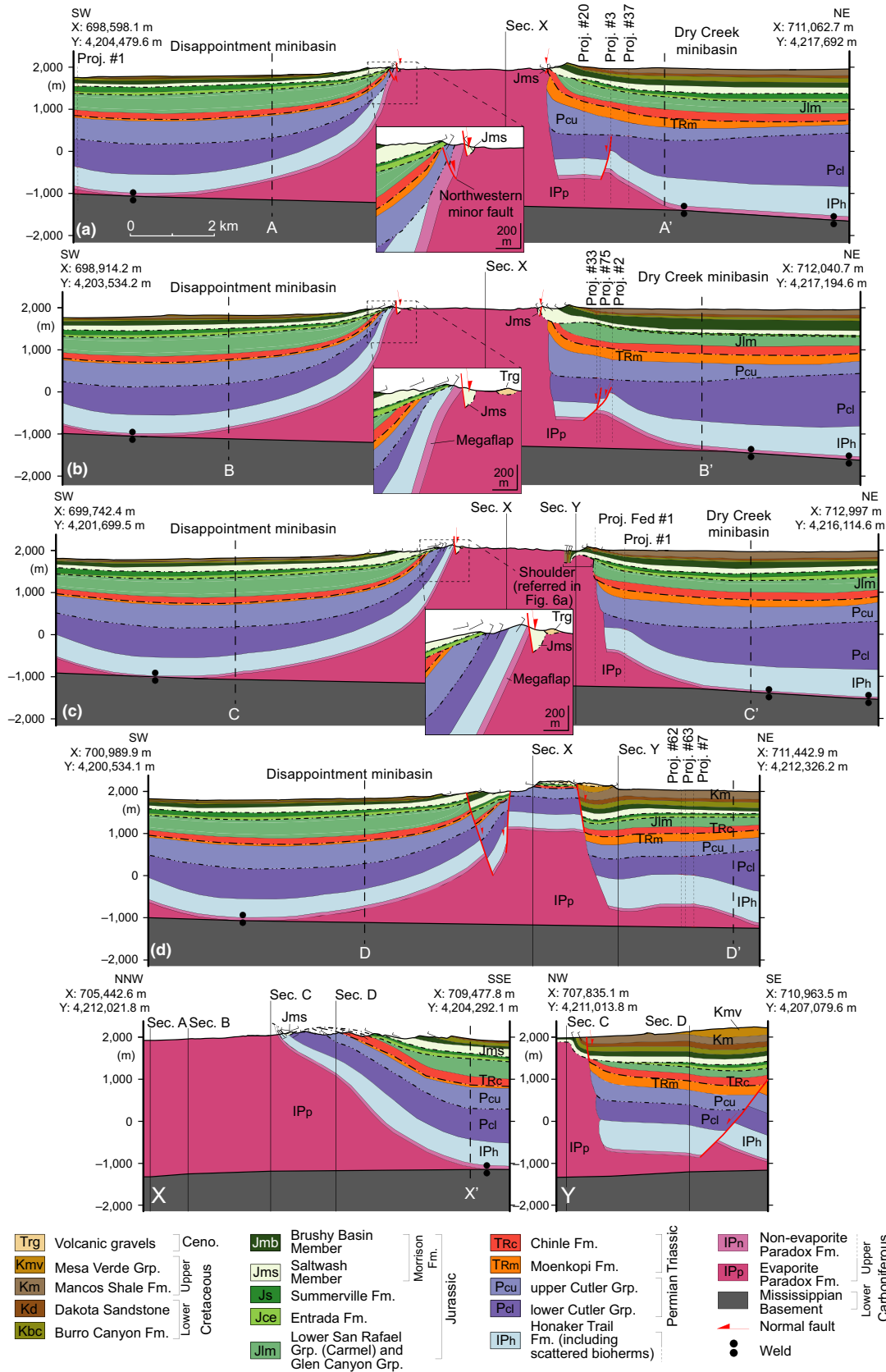


FIGURE 7 Geologic cross sections constructed using surface and sub-surface data (locations in Figures 4 and 6). Vertical dashed lines marked by A–A', B–B', C–C', D–D' and X–X' indicate the limits of the geological map shown in Figure 4, vertical solid lines denote the intersections with other cross sections and vertical fine dashed lines indicate wells within 200 m of the cross sections. Stratigraphic colours, labels and unconformity styles as in Figures 2 and 4

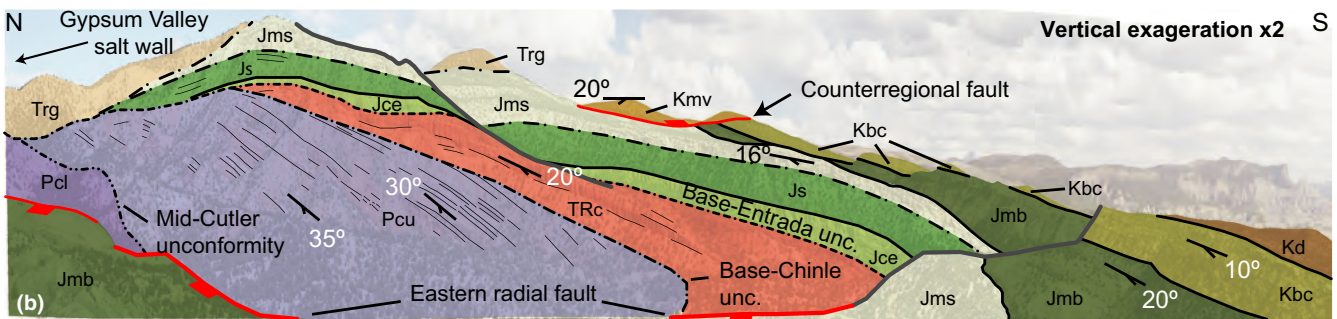
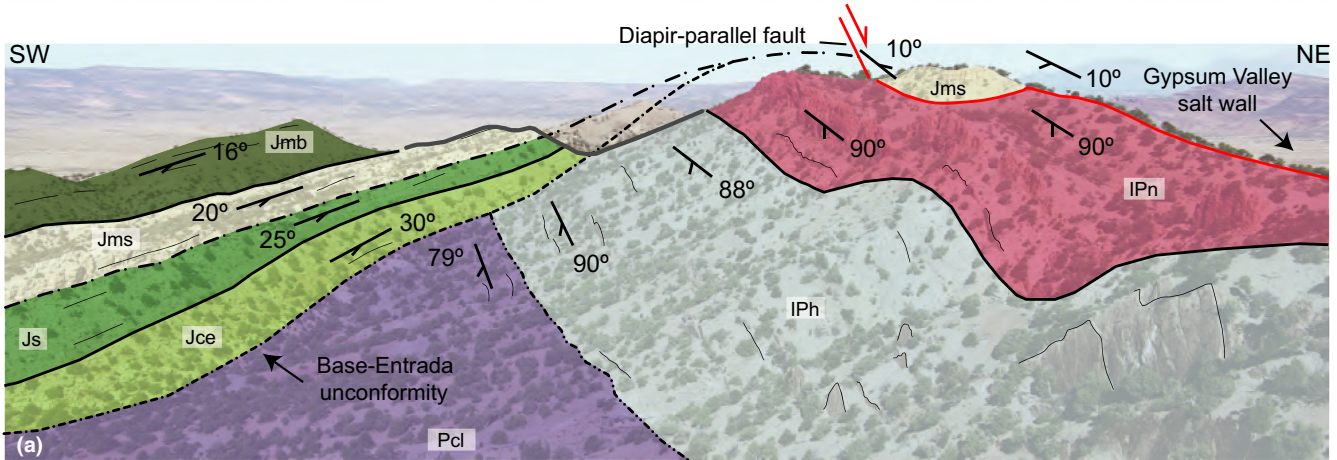


FIGURE 8 (a) Interpreted photo panorama of the megaflap (nonevaporite Paradox Fm., Honaker Trail Fm. and lower Cutler Grp.) and strata above the capping base-Entrada unconformity (Entrada Fm., Summerville Fm. and Morrison Fm.) in SD I'. (b) Interpreted photo panorama of the strata overlying the southeastern termination of the salt wall (SD III). See the location of the photo panoramas in Figure 4. Stratigraphic colours and labels as in Figures 2 and 4. Thin black continuous lines – bedding traces; dot-dashed lines – main unconformities; thick black continuous lines – concordant contacts; red lines – faults; grey lines – topographic mountain profile

Radial faults

Strata flanking the diapir at its southern corner are cut by the western and eastern radial faults (2.9 and 3.5 km long respectively). They are approximately orthogonal to the diapir edge, diverge away from the diapir, and bound a down-dropped block (Figure 4 and 6a). The N-S trending western fault dips towards the NE and has an estimated throw of *ca.* 480 m on section D (Figure 7) and the NW-SE to NNE-SSW trending eastern fault dips towards the SW and has an estimated throw of *ca.* 400 m (Figure 4 and 7, section D). Both radial faults decrease in throws southwards away from the diapir until they terminate within the Mancos Shale.

Counterregional fault

A large, NW-SE trending, down-to-the-NE normal fault extends away from the southeastern termination of the Gypsum Valley salt wall (Figure 4 and 7, section D). Because its geometry is analogous to that of counterregional (landward-dipping) faults in the northern Gulf of Mexico, in that it dips towards the source of prograding sediment and curves into the proximal edge of the diapir (Diegel, Karlo, Schuster, Shoup, & Tauvers, 1995; Schuster, 1995), we apply the same terminology. The counterregional fault accommodates more than 1.5 km of throw close to the salt wall, with Honaker Trail Fm. in the footwall and a thickened Upper Pennsylvanian to Cretaceous sequence in its hanging wall (Figure 7, section D). Displacement decreases away from the diapir to the SE (Figure 4).

Lateral fault

Northeast of where the counterregional fault merges with the diapir is a small, NE-SW trending, down-to-the-SE normal fault (Figure 6a) within the Dakota Sst. Slickenlines plunge 24° and 40° towards 150 and 171, respectively (i.e. NNW-SSE-oriented oblique slip). We do not term this a radial fault because radial faults merely segment drape-folded strata, whereas this fault separates two very different structural domains (see below).

Diapir-parallel faults

Along both outer edges of the diapir are steep normal faults oriented parallel to the salt wall margin (Figures 4 and 6a). The hanging walls have Morrison Fm. strata down-dropped directly onto the Paradox Fm. evaporites (Figure 7, sections A–C insets).

3.3.2 | Structural domains

Diapir-flanking strata around the southeastern termination of the Gypsum Valley salt wall are divided into five SD separated by some of the faults described above (Figure 6a).

SD I

The southwestern flank of the Gypsum Valley salt wall (SD I) is dominated by the megaflap (Figures 6a and 8a). It is subdivided into two sub-domains (SD I' and SD I''), separated by the northwestern minor fault (Figures 4 and 6a), according to the character and amount of internal deformation observed within the megaflap, as described below. In addition to the megaflap, another common element is the diapir-parallel normal faults that juxtapose low-dipping Morrison Fm. above the diapir against vertical megaflap strata adjacent to the diapir (Figures 4 and 7, sections A–C).

Although SD I'' is southeast of SD I', it is described first because it has a simpler character. It is equivalent to Zone 1 of Mast (2016), where the megaflap is composed of two mechanically differentiated but concordant units: (a) an upper unit formed by the Honaker Trail Fm. carbonates and siliciclastics and the lowermost part of the lower Cutler Grp. carbonates; and (b) a lower unit made up of carbonates interbedded with mudstones of the Paradox Fm. (probably corresponding to the uppermost Ismay informal Mbr., Deatrick et al., 2015; Mast, 2016). In other words, the nonevaporite uppermost part of the salt diapir is part of the megaflap.

The megaflap decreases in dip south-eastward, from near-vertical to overturned in the northwestern part of SD I'' to about 60° close to the western radial fault (Figure 4). Above the mid-Cutler unconformity, the upper Cutler Grp. through Lower Jurassic strata form a growth wedge that is truncated beneath the 30–35° dipping base-Entrada unconformity (Figures 4, 7 sections B and C, and 8a). The entire structure (megaflap and capping unconformity) deepens along strike to the northwest so that only the nonevaporite member of the Paradox Fm. is exposed between the unconformity and diapir near the boundary with SD I' (Figure 4). The fold axis of the megaflap drape fold plunges 7° towards 264°, slightly oblique to the 255° trend of the diapir edge (Figure 6b).

SD I', like the northwestern part of SD I'', exposes only the uppermost Ismay Mbr. of the Paradox Fm. between the diapir and the mid-Cutler unconformity (Figures 4 and 7, section A). Just NW of the northwestern minor fault (Zone 2 of Mast, 2016; Figure 6a), however, it is characterized by discontinuous dolomite ridges that form short-wavelength, low-amplitude asymmetric folds interbedded with black shales. Fold axes are sub-horizontal (*ca.* 3°–15° plunge) and roughly parallel to the edge of the diapir and the fold axis of the megaflap panel (Figure 6b). Longer fold limbs are near vertical and shorter limbs dip *ca.* 70° to the SW, suggesting a NE-side-up sense of shear.

The uppermost Ismay Mbr. in Zone 3 of Mast (2016), at the northwestern end of the megaflap in SD I' (Figure 6a), contains discordant dolomite blocks. The lithology

is similar to Zone 2 of Mast (2016) and folds are still recognized, but the dolomite blocks appear to be isolated and encased in black shales and marls. Thus, the oldest strata in the megaflap become increasingly deformed towards the NW: they are conformable, without significant internal deformation, in SD I'; they include coherent asymmetric folds in southeastern SD I'; and they are disrupted in northwestern SD I'.

There is no evidence for any structural thinning of the Honaker Trail Fm. and the lowermost part of the lower Cutler Grp. during stratal rotation (Rowan et al., 2016). In addition, well control shows that the Honaker Trail Fm. at the base of the Disappointment minibasin has a thickness intermediate between that within the megaflap and that at the base of the Dry Creek minibasin.

SD II

SD II is the graben bounded by the two large radial faults at the southern corner of the diapir (Figure 6a). Bedding dips are a maximum of ca. 65° to the SSW near the diapir and gradually decrease southward. Jurassic strata in the northern part of the graben (Figure 4) are folded into a low-amplitude anticline-syncline pair with sub-horizontal fold axes trending roughly parallel to the eastern bounding fault (Figure 6b). The Brushy Basin Mbr. to Dakota Sst. are ca. 150 m thicker within the graben (Figure 7, section D); older strata are not exposed.

SD III

SD III, located off the southeastern termination of the salt wall, is bounded by the eastern radial fault to the W and the counterregional fault to the NE (Figures 6a and 8b). Strata in SD III form a moderately to gently dipping panel over the plunging nose of the diapir (Figure 7, section X), with maximum dips (45°) close to the diapir (Figures 4 and 6b). Within SD III, the mid-Cutler unconformity progressively cuts out more strata closer to the counterregional fault and the base-Entrada unconformity cuts out more section approaching the diapir (Figures 7, section X and 8b).

SD IV

SD IV forms the hanging wall of the counterregional fault (Figure 6a). Strata are generally sub-horizontal (Figure 7, sections D and Y), but a broad, gentle syncline with a fold axis plunging 5° towards 112° probably intersects the counterregional fault near its termination against the diapir (Figures 4 and 6b). SD IV is bounded to the NW by SE-dipping strata cut by the lateral fault (Figure 7, section Y).

SD V

SD V is located along the northeastern flank of the salt wall (Figure 6a). Strata in the Dry Creek minibasin are folded within 2 km of the diapir, with dips as steep as 80°

immediately adjacent to the salt structure (Figure 7, sections A–C). Along most of its length, SD V is bound to the SW by a SW-dipping normal fault with Morrison Fm. strata in its hanging wall adjacent to exposed diapir caprock (Figure 4). The fault dies out towards the SE and is replaced by a SE-plunging asymmetric anticline with a gently-dipping (ca. 20°) NE limb and a steep (ca. 80°) SW limb (Figures 4 and 6b). The fold-axis plunge increases to ca. 60° near the termination of the salt wall, with the SE-dipping strata offset slightly by the lateral fault (Figures 4 and 7, section Y).

4 | SUMMARY AND INTERPRETATION

The stratal geometry flanking Gypsum Valley diapir is asymmetric, whereas strata on the SW flank are depositionally thinned and folded to near-vertical in the megaflap, strata on the NE side are thicker, deeper and mostly gently dipping. The asymmetry continues off the southeastern end of the diapir, where the counterregional fault separates SDs III and IV. This style is typical of counterregional systems (Rowan & Inman, 2005; Schuster, 1995), where differential minibasin subsidence is accommodated by a combination of the diapir (Figure 7, sections A–C) and counterregional faults extending off its ends (Figure 7, section D). At the diapir, slip is likely to have been accommodated by shear within the salt, not by a discrete fault at its edge. Because the Honaker Trail Fm. is thin in the footwall of the counterregional fault and along the southwestern flank of the diapir, and thicker in the hanging wall and along the northeastern flank, the asymmetry and counter-regional-style relationship were established from the onset of salt movement (Figure 5). The style of diapirism was that of single-flap active diapirism (Schultz-Ela et al., 1993), not reactive rise.

4.1 | Southwest (high) side

There are significant along-strike changes in geometry on the southwestern, upthrown side of the diapir and counterregional fault. The most prominent is the existence of the radial faults and intervening graben (Figures 4 and 6a). These were probably caused by drape folding around a curved edge of salt and the resultant concentric tensile (hoop) stress regime (Coleman, Jackson, Duffy, & Nikolianakou, 2018; Rowan et al., 2003; Stewart, 2006; Figure 9). Indeed, the radial faults are located exactly where the strike direction of the diapir edge and adjacent Honaker Trail Fm. strata changes most abruptly (Figures 4 and 6a). The concentration of radial faults at the ends of the salt wall is compatible with observations from the North Sea (Davison

et al., 2000; Stewart, 2006). The minor folds within the graben are more enigmatic. They may have formed due to crowding as the wider younger section was dropped down into a narrower space (Figure 9); alternatively, they may have formed during late (Laramide) contraction. The onset and duration of radial faulting is unknown, except that the faults were active as late as during deposition of the Mancos Shale Fm. Because they presumably formed due to drape folding, they were probably long-lived since differential salt evacuation/diapirism began during Honaker Trail deposition (Figure 5). They would have grown in displacement with increased folding and would gradually have propagated away from the diapir (Figure 9). The fault lengths and net displacement may have increased due to late reactivation during the Laramide contraction.

The geometry of the Honaker Trail Fm., and thus probably the salt–sediment interface, changes as the termination of the diapir is approached. The strata are steep, approaching vertical, along the elongate SW side (Figures 3 and 7, sections A–B), but gradually decrease towards the SE (Figure 7, section C), so that the diapir termination forms a plunging nose over a distance of about 4 km (Figure 7, section X). Because megaflaps are defined as having near-vertical to overturned dips (Rowan et al., 2016), the Gypsum Valley megaflap terminates gradually to the SE as the dips decrease near the western radial fault (Figure 4), and there is no megaflap at the structural nose of the salt wall termination. This gradual termination and decrease in dip may be related to the deep salt budget since limb rotation to vertical in halokinetic megaflaps requires an adequate thickness of deep salt (Rowan et al., 2016). Thus, beneath the Gypsum Valley megaflap, the salt would have been thick enough for strata to rotate to vertical, but rotation was limited where the salt might have thinned southeastward towards the edge of the basin (Figure 1a).

The style of megaflap termination to the NW is uncertain. Maximum dips of the megaflap strata are slightly decreased in SD I' (65–80°) and the strata are buried beneath the Morrison Fm. farther NW. Seismic data show that the megaflap is absent 13 km to the NW, with the Honaker Trail Fm. truncated at depth beneath the mid-Cutler unconformity (Figure 3a). Whether the megaflap gradually decreases in dip and elevation, or is truncated abruptly by one or more faults, is unknown.

As described above, the uppermost Paradox Fm. black shales and interbedded carbonates are parallel to the Honaker Trail Fm. in SD I', but the latter are folded in the southeastern part of SD I', and completely disrupted to the NW. The asymmetric fold geometries suggest formation during roughly diapir-parallel shear, with a sense of motion of the inside of the diapir up relative to flanking strata in the minibasin. Two possible origins for this deformation are considered. First, the deformation might have occurred

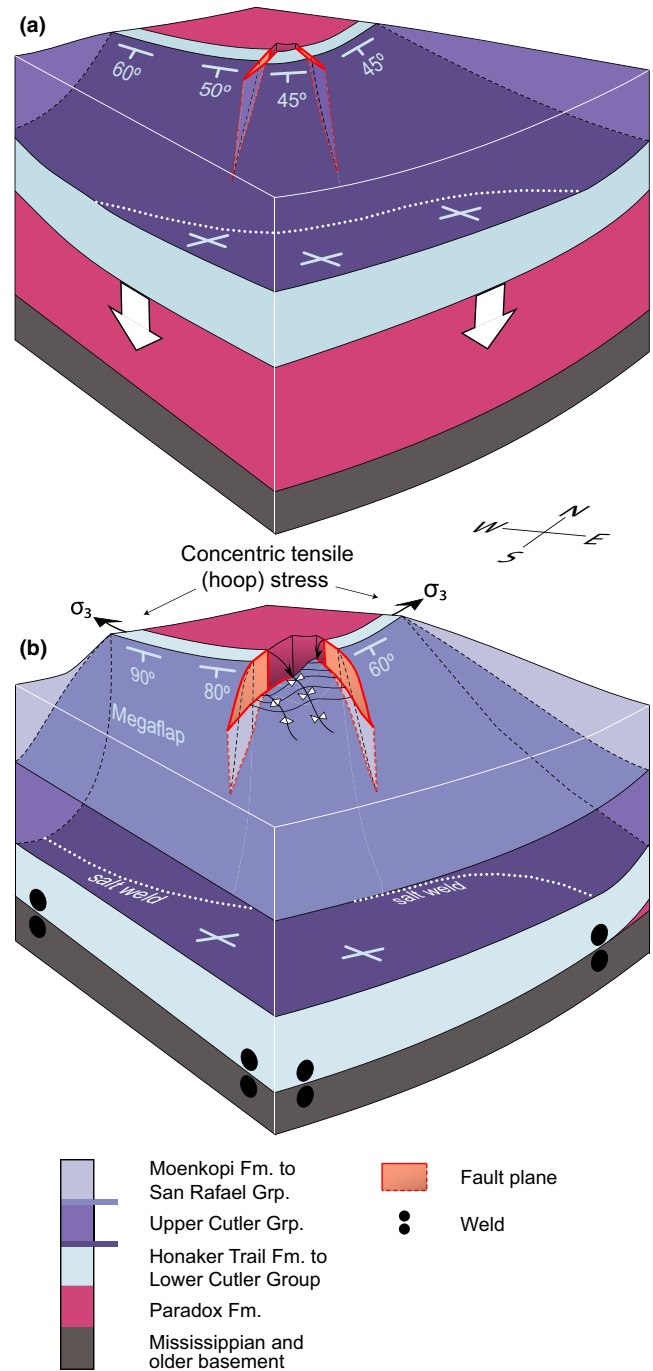


FIGURE 9 Block diagrams showing the evolution of the radial faults at the termination of Gypsum Valley salt wall: (a) earlier drape fold stage; and (b) later stage with strata rotated to vertical in megaflap

early as soft-sediment deformation during the earliest inflation of the diapir just to the NE. In this case, the deformed and disrupted strata would still be considered part of the megaflap, simply rotated during drape folding. Alternatively, the deformation could have been caused at any time by ductile flow of the salt and associated weak shales, in which case the uppermost Paradox in this area acted as part

of the diapir, not the megaflap. One implication of this latter interpretation is that the base of the megaflap can shift stratigraphically along the edge of the diapir.

4.2 | Northeast (low) side

There is relatively minor along-strike variation in the large-scale geometry of the northeastern, downthrown flank of the diapir (Figures 4 and 7). One difference is that the Mesozoic strata climb gently towards the diapir over a zone about 1.5–2 km wide within SD V (Figure 7, sections A–C), the same strata in the hanging wall of the counterregional fault (SD IV) are sub-horizontal (Figure 7, section D). The required change in elevation occurs right at the SE termination of the diapir, manifested by the local SE-dipping Dakota Fm. strata, the minor lateral fault, and the presence of the Mesa Verde Grp. only to the SE (Figures 4 and 7, section Y).

Is this change in elevation due to ongoing drape folding adjacent to the diapir during the Late Cretaceous or to some other factor, and is the lateral fault separating SD IV and V just a radial fault due to drape folding? We have already pointed out that there is no drape fold to the SE of the fault, so that it is unlikely to be a radial fault. To the NW of the fault, there are two scales of folding: gentle folding of the Dakota Sst. and younger strata extending close to 2 km from the salt (Figure 7, sections A–C); and a narrower zone of folding within the underlying Morrison Fm., as indicated by a sudden increase in dip, within about 300 m of the diapir on section B (Figure 7). The latter is compatible with halokinetic folding, which occurs within 1 km of a passive diapir (Giles & Rowan, 2012). Moreover, the regional level of the top Dakota Sst. (defined as the level where the strata have not gone up or down due to local deformation; Hossack, 1995) is consistent over a broad area along the eastern portions of sections A–D and most of section Y (Figure 7). In contrast, the Dakota Sst. within the 1.5–2 km wide zone of folding is above regional. Thus, we attribute the near-diapir folding to a combination of two processes. The more pronounced folding occurring within 300–500 m of the diapir likely represents halokinetic drape folding during ongoing passive diapirism in the Jurassic. However, we infer that the broader zone of gentler folding, recorded by the Burro Canyon Fm. and Dakota Sst., was generated by minor diapir rejuvenation during the subsequent Laramide Orogeny. The amount of shortening decreasing abruptly at the end of the salt wall, accommodated in part by a lateral tear fault.

Another change in near-diapir deformation on the NE flank of the diapir is that a normal fault dipping towards the diapir transitions to the SE to an anticline with a steeper limb on the diapir side (Figure 4). The tightness of the fold cannot be explained by deformation above the deep

salt level and thus suggests the presence of an inward stepping of the diapir edge (i.e. salt shoulder) that was progressively overlapped by Morrison Fm. strata (Figure 7, sections C and Y). Both the diapir-parallel normal fault and the fold are interpreted as different manifestations of shoulder collapse due to halite dissolution and the formation of caprock (see McFarland, Giles, Langford, & Rowan, 2015).

5 | DISCUSSION

In the following sections, we compare the southeastern termination of Gypsum Valley salt wall, with its counterregional fault, firstly to other diapir terminations in the Paradox Basin and secondly to similar features in the northern Gulf of Mexico. We then discuss general aspects of salt wall and megaflap terminations.

5.1 | Paradox Basin salt wall terminations

Four other diapirs (shown in Figure 1a) have known similarities to the Gypsum Valley diapir (Table 1). First, the Onion Creek diapir has a megaflap on the distal (SW) side (Hudec, 1995; Trudgill, 2011), but no counterregional faults are mapped. Second, the Castle Valley diapir has no megaflap, although a 300 m long and N-S trending counterregional (E-dipping) structure extending away from its NW end has been identified as a salt weld, not a fault (Lawton et al., 2015). Welding was presumably caused by some combination of NE side subsidence, dissolution, and late contraction. Third, the nearby Moab Valley diapir extends in the subsurface for over 20 km NW from the surface termination as a salt roller in the footwall of the NE-dipping Moab fault. This fault was active during late (Cenozoic) extension and/or salt dissolution (Pevear, Vrolijk, & Longstaffe, 1997; Solum, van der Pluijm, & Peacor, 2005; Trudgill, 2011; Trudgill, Banbury, & Underhill, 2004), but an early origin as a counterregional fault is uncertain. Finally, the Lisbon Valley diapir is an inflated salt roller in the footwall of a 20-km long counterregional fault (Morrison & Parry, 1986; Parker, 1981). The slightly asymmetric geometry of its flanking minibasins demonstrates that fault activation occurred early (Fleming, 2015); it may have been analogous to the early single-flap active diapir phase at Gypsum Valley diapir (Figure 5b). However, the Lisbon Valley salt never broke through to grow as a passive diapir, but was simply reactivated during late contraction and extension (Fleming, 2015).

We highlight these aspects of other salt walls to show that there are both similarities and differences between their geometries and those described here for the Gypsum Valley salt wall. The comparison is intriguing, and suggests that

TABLE 1 Selected attributes of different salt walls within the Paradox Basin derived from the literature (information for salt walls other than Gypsum Valley taken from Banbury, 2005; Fleming, 2015; Hudec, 1995; Lawton & Buck, 2006; Lawton et al., 2015; Morrison & Parry, 1986; Parker, 1981; Trudgill, 2011)

	SE Gypsum Valley	SW Onion Creek	NW Castle Valley	NW Moab Valley	Lisbon Valley
Type	Salt wall	Salt wall (Fisher Valley)	Salt wall	Salt wall	Salt roller
Structural relief (m)	2,300	3,800	3,000	2,500	2,700
Timing of diapirism	Pennsylvanian to Jurassic	Pennsylvanian to Permian	Pennsylvanian to Early Triassic	Pennsylvanian to Triassic	Pennsylvanian, Cenozoic
Major bounding structure	Counterregional fault	Is not mapped	Counterregional weld	Late extensional fault	Late extensional fault
Geometry of flanking minibasins	Asymmetric	Asymmetric	Asymmetric	Slightly asymmetric	Slightly asymmetric
Salt wall termination geometry	Steep plunging nose	Steep plunging nose	Steep plunging nose	Gradual plunging salt roller	Gradual plunging salt roller
Salt wall attenuation distance (km)	Short (4)	Short (3.1)	Short (1.6)	Long (20)	Short to moderate (8)
Megaflap	Yes	Yes	No	Yes	No
Radial faults	Yes	Are not mapped	Yes	No	No

further work is warranted in order to understand better the styles and processes of diapirism and salt–sediment interaction in the Paradox Basin.

5.2 | Counterregional systems in the northern Gulf of Mexico

Counterregional faults extending away from diapir terminations are also known from the northern Gulf of Mexico (Diegel et al., 1995; Rowan & Inman, 2005; Rowan, Jackson, & Trudgill, 1999; Schuster, 1995; Trudgill & Rowan, 2004). They are found above both the autochthonous and allochthonous salt levels, the diapirs are often basinward-leaning rather than vertical, sub-circular stocks are more common than salt walls, and megaflaps have not been reported.

The oldest strata on the downthrown side at Gypsum Valley diapir are thicker than on the upthrown side. Similar relationships exist in the northern Gulf of Mexico (Schuster, 1995, figures 10 and 11; Trudgill & Rowan, 2004, figure 7b). In other cases, the opposite relationship exists, with the oldest strata in the proximal minibasin being thinned and the younger section being thicker (Rowan & Inman, 2005, their figure 1). The same geometry is seen at Salt Valley diapir in the Paradox Basin (Trudgill, 2011, figure 5a) indicating both styles can exist in the two basins. The difference in style is related to the early style of salt rise and the position of diapir breakthrough. If the roof is unfaulted and the salt simply inflates, progressive loading on the proximal side leads to diapir breakout at the distal

end of the inflated salt, with the thinned oldest strata (the roof of the early inflated salt) ending up at the base of the landward minibasin (Figure 10a). If, in contrast, the early history is that of single-flap active diapirism, with the fault and eventual diapir breakthrough located at the proximal end of the inflated salt, the thinned roof (flap) ends up draped on the distal side of the diapir, potentially as a megaflap (Figure 10b). Of course, the geometry may change from one style to the other along strike, possibly due to variations in roof thickness and strength, thereby providing one possible form of megaflap termination.

In counterregional-style systems of the northern Gulf of Mexico, the largest differential subsidence is centred adjacent to the diapirs (Rowan & Inman, 2005). Differential subsidence may still be significant along strike from the diapirs, where it is taken up by slip on counterregional faults that merge into the proximal edges of the diapirs (Rowan & Inman, 2005; Rowan et al., 1999; Trudgill & Rowan, 2004). Note that this model requires no regional extension to be accommodated by the faults (Schuster, 1995). The deeper portions of the faults are actually welds since the salt evolves from linear, low-relief walls to high-relief stocks (Trudgill & Rowan, 2004). As fault displacement decreases along strike, the differential subsidence is increasingly accommodated by folding, until only monoclinical folding records the deformation around the landward and lateral margins of the minibasin. This is similar to the geometry observed at the southeastern termination of the Gypsum Valley salt wall, where the counterregional fault emanates from the proximal edge of the diapir,

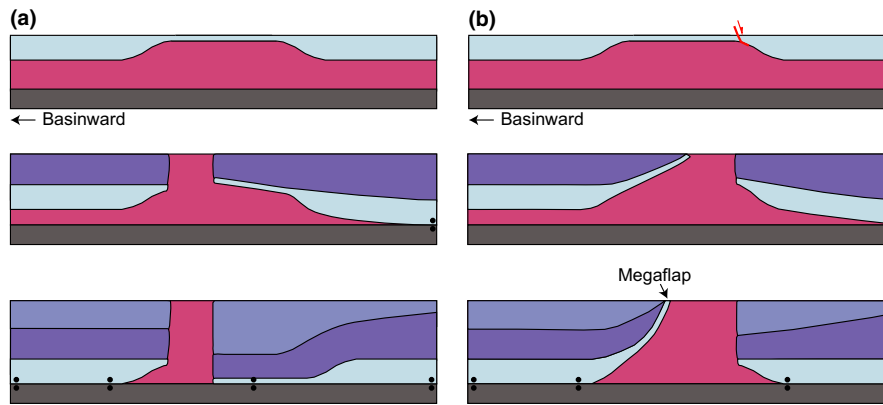


FIGURE 10 End-member scenarios for the evolution of counterregional-style diapirs (based in part on Rowan & Inman, 2011; Rowan et al., 2016): (a) early salt inflation due to progressive depositional loading, with salt breakout at the basinward edge of the inflated salt; (b) early single-flap active diapirism (Schultz-Ela et al., 1993), with salt breakout at the proximal edge of the diapir and development of a megaflap along the basinward flank of the diapir

accommodates differential subsidence of the two minibasins, and decreases in displacement away from the diapir.

5.3 | Salt wall and megaflap terminations

In general, structures extending off the terminations of salt walls differ depending on the local tectonic setting. They may be contractional salt-cored anticlines, thrust faults, extensional faults, strike-slip faults, or counterregional faults related to differential salt evacuation. However, we focus here only on passive diapirism driven by differential loading, without significant regional extension or contraction, and specifically on the final geometry after the flanking minibasins have touched down to form welds. We first address the termination geometry of the diapir itself (with or without a megaflap, Figure 11), then cases in which the salt wall and megaflap terminations are coincident (Figure 12), and finally cases in which a halokinetic (noncontractional) megaflap terminates away from the end of the salt wall (Figure 13).

The geometry of the termination of a passive salt wall is ultimately controlled by the available salt budget and the patterns of sedimentary loading, and thus the spatial variations in salt evacuation and flow towards the diapir. If, for example, the autochthonous salt basin has an abrupt lateral boundary (such as a basement-involved fault), a salt wall formed near the basin edge will have an equally abrupt termination, with flanking depocentres bounded by steep faults separating the subsiding minibasins from areas of no corresponding subsidence off the end of the diapir (Figure 11a). If there is no local variation in deep salt thickness to begin with, the salt wall is liable to plunge along strike and its edge will have a curved map-view outline, with depocentres on all sides and radial faults best developed

where curvature of drape-folded strata is greatest (Figure 11b). The salt budget for flow into the diapir from beneath the depocentres will be controlled in part by the position of nearby diapirs and thus the fetch area for deep salt.

The cartoons in Figure 11a, b show symmetric diapir flanks, but diapirs may be slightly to highly asymmetric. If asymmetric, the diapir may be associated with a counterregional fault at one corner, radial faults on the other corner, and a possible megaflap (Figure 11c), as observed at Gypsum Valley. Note that although the corner where the counterregional fault intersects the diapir is broadly curved, no significant radial faults form because there is no curved drape fold. The diapir termination may be relatively abrupt, in which case differential subsidence is high immediately adjacent to the end of the salt wall but decreases rapidly along strike away from the diapir, the top salt correspondingly plunges relatively steeply, radial faults are well developed due to high degrees of map-view curvature of the flanking strata, and the counterregional fault or equivalent weld is relatively short (Figure 12a). Alternatively, the salt wall termination may be gradual, with differential subsidence diffused over a broader area, a gently plunging salt nose, less map-view curvature and thus less common radial faults and a longer counterregional fault (Figure 12b). The difference might again be explained by the deep salt budget: if it decreases rapidly along strike, the termination will be more abrupt and radial faults will be common (Figure 12a); otherwise, the termination will be gradual and radial faults absent or minor (Figure 12b). The SE termination of the Gypsum Valley diapir falls between these end-member geometries.

Megaflaps may also terminate before reaching the end of a salt wall. Because megaflaps are defined by the

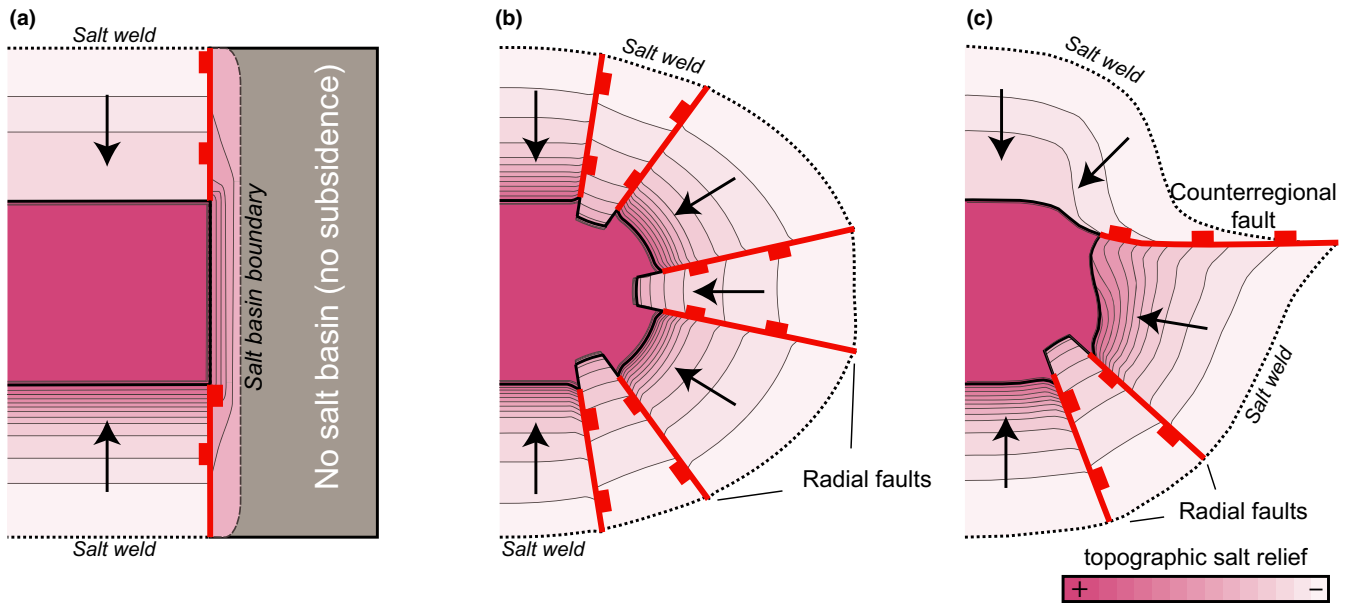
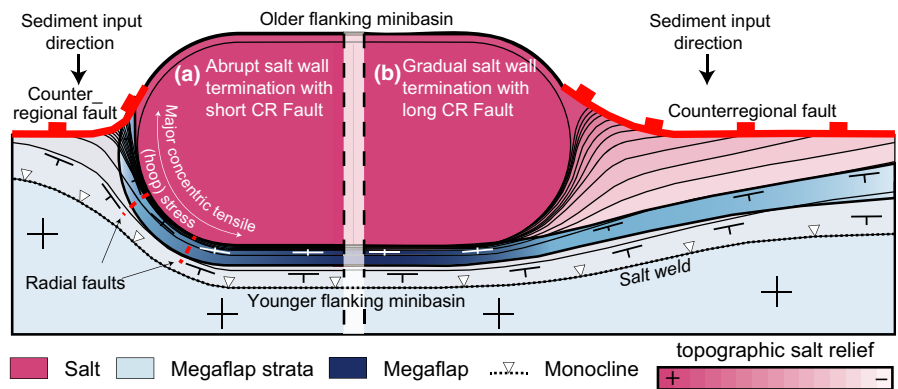


FIGURE 11 Schematic illustrations of end-member termination geometries of salt walls (red faults are all suprasalt, contour lines are on top salt): (a) symmetric salt wall termination above a presalt basement fault (not shown); (b) symmetric salt wall termination where there is deep salt present off the end of the diapir; (c) termination where the salt wall is asymmetric, with a counterregional fault off the end. Note that radial fault development depends on both map-view curvature and the degree of drape folding of flanking strata. Arrows indicate salt flow into diapir

FIGURE 12 Schematic plan view of varying terminations of salt walls with asymmetric minibasins and megaflaps. Red dashed lines indicate radial faults; red continuous lines indicate the counterregional fault at (a) abrupt and (b) gradual salt wall terminations; continuous black lines indicate topographic contours on the top salt



steepness and height of the stratal panel, end-member styles of termination are a gradual decrease in elevation or maximum dip of the megaflap panel along strike or an abrupt drop or decrease in dip across one or more faults (Figure 13). Combinations of any of these are possible and likely in natural examples. One possible cause for lateral termination is a decrease in deep salt budget along strike, as suggested above for the Gypsum Valley megaflap; again, a megaflap forming by limb rotation cannot reach vertical if the salt is too thin relative to the rotating roof panel (Rowan et al., 2016). A second factor is the width of the early pillow or single-flap active diapir; as the width decreases, there is less roof length available to rotate into steep attitudes. Similarly, a third factor is any lateral variation in where the roof pulls apart and salt breaks through. If the early fault that separates the strata that end up on

one or the other sides of the diapir is consistently along one edge of the early salt structure, then the geometry of a megaflap will change very little along strike (for a constant width early pillow). If, however, the fault gradually or abruptly crosses the top of the pillow, the length of the roof panel that rotates into the megaflap is diminished and the rest of the roof ends up flanking the other side of the diapir (assuming none is removed by erosion).

6 | CONCLUSIONS

The Gypsum Valley diapir is an outstanding natural laboratory for studying the three-dimensional architecture of the terminations of both a salt wall and a megaflap. From this example, and from comparison to analogous structures in

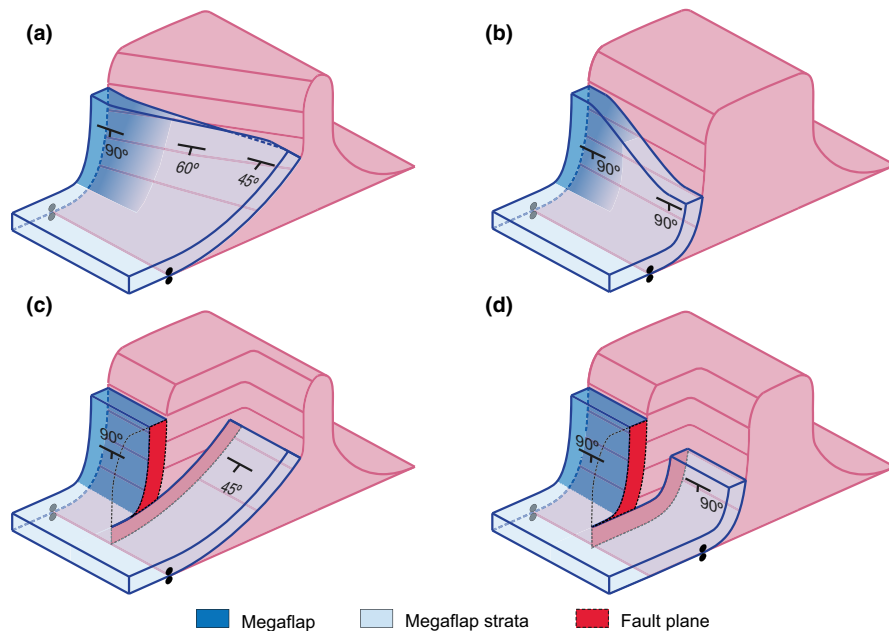


FIGURE 13 End-member styles of megaflap termination along the length of a salt wall: (a) constant limb length with gradual decrease in dip along strike; (b) gradual decrease in limb length with constant dip along strike; (c) constant limb length with abrupt decrease in dip across a fault; (d) abrupt decrease in limb length with constant dip across a fault. These are conceptual models of end-member geometries; most real examples combine elements of these

the Paradox Basin and the northern Gulf of Mexico, we have demonstrated or suggested the following:

1. The southeastern end of the Gypsum Valley salt wall is asymmetric, with thicker, deeper, gently dipping strata in the proximal NE minibasin and thinned, rotated older strata forming a megaflap on the distal SW side. Its termination is characterized by a moderately plunging nose of salt overlain by SE-dipping strata with maximum 45° dips, a large counterregional fault that separates the nose from the deep proximal minibasin, and radial faults that accommodate concentric extension where the map-view curvature of the flanking strata is greatest.
2. The megaflap, which is characterized by near-vertical strata, terminates towards the southeastern end of the diapir by a decrease to ca. 60° dips over a distance of several hundred metres before being truncated by the western radial fault. The northwestern termination is buried by younger strata. The megaflap includes undeformed nonevaporite strata of the uppermost Paradox Fm. to the SE, but this same interval becomes increasingly deformed along strike to the NW. This deformation may represent early syn-sedimentary slumping or part of the intrasalt deformation; in the latter case, the base of the megaflap would change stratigraphic position along strike.
3. In counterregional systems like the Gypsum Valley diapir and possibly analogous structures in the northern Gulf of Mexico, megaflap formation on the distal flank is favoured when the salt breaks out on the proximal side of the initial salt pillow or diapir.
4. In general, salt wall terminations may be abrupt or gradual. Controlling factors probably include the spatial and thickness variation in the deep salt, the presence of nearby diapirs and thus the fetch area for salt feeding the wall, and the pattern of depositional loading and associated flow of salt into the diapir.
5. For a salt wall without significant extension or contraction, if the two flanking minibasins are highly asymmetric, a counterregional fault extends off the end of the wall. The length of the counterregional fault away from the diapir depends in part on the degree of plunge of the salt wall nose.
6. Megaflaps may terminate at any position along the salt wall. Termination is accommodated by decreased length and/or dip of the megaflap strata that occurs either gradually or abruptly at one or more faults. Controlling factors include the deep salt budget, the width of the initial salt pillow or single-flap active diapir and variations in the position on the early salt structure at which the roof separates and the salt breaks out.
7. In all cases, radial faults will be most prevalent where there is the maximum map-view curvature of drape-folded strata. They tend to have more offset and extend farther from the diapir with wider zones and higher degrees of stratal upturn, as found in megaflaps.

ACKNOWLEDGEMENTS

This work has been supported by projects SALTECRES (CGL2014-54118-C2-1-R) and 2014SGR467 at the University of Barcelona and the Salt-Sediment Interaction Research Consortium at The University of Texas at El Paso, funded by BP, BHP, Chevron, ConocoPhillips, ExxonMobil, Hess, Kosmos, Repsol, and Shell. The University of Barcelona is acknowledged for a PhD fellowship (APIF) for the first author. The authors wish to

acknowledge Cynthia Ebinger, Chris Talbot, and Chris Jackson for their helpful reviews which greatly contributed to improving the final product. We thank Mark Fischer and Gary Gianniny for helpful discussions on salt–sediment interaction and all the people who helped the first author in numerous field campaigns. We also acknowledge Midland Valley for providing the Move™ software.

ORCID

Frederic O. Escosa  <http://orcid.org/0000-0002-1908-1037>

REFERENCES

- Amador, C. M., Schurger, S. G., & Miller, B. L. (2009). Andy's Mesa Unit, San Miguel County, Colorado. In W. S. Houston, L. L. Wray & P. G. Moreland (Eds), *The Paradox Basin revisited-New developments in petroleum systems and basin analysis: Denver, Colorado* (pp. 497–518). Denver, CO: Rocky Mountain Association of Geologists, 2009 Special Publication.
- Baars, D. L. (1965). *Pre-Pennsylvanian paleotectonics of southwestern Colorado (San Juan County and vicinity) and east-central Utah*. PhD Thesis, University of Colorado, Boulder, CO.
- Baars, D. L., & Stevenson, G. M. (1981). Tectonic evolution of the Paradox basin, Utah & Colorado. In D. L. Wiegand (Ed.), *Geology of the Paradox basin: Denver Colorado* (pp. 23–31). Denver, CO: Rocky Mountain Association of Geologists.
- Balkwill, H. R., & Legall, F. D. (1989). Whale Basin, offshore Newfoundland: Extension and salt diapirism. In A. J. Tankard & H. R. Balkwill (Eds), *Extension tectonics and stratigraphy of the North Atlantic margins. American Association of Petroleum Geologists Memoir 46*, 233–245.
- Banbury, N. J. (2005). *The role of salt mobility in the development of supra-salt sedimentary depocentres and structural style*. PhD Thesis, University of Edinburgh, Edinburgh, UK.
- Barbeau, D. L. (2003). A flexural model for the Paradox basin: Implications for the tectonics of the Ancestral Rocky Mountains. *Basin Research*, 15, 97–115. <https://doi.org/10.1046/j.1365-2117.2003.00194.x>
- Blakey, R. C. (2009). Paleogeography and Geologic History of the Western Ancestral Rocky Mountains, Pennsylvanian-Permian, southern Rocky Mountains and Colorado Plateau. In W. S. Houston, L. L. Wray & P. G. Moreland (Eds), *The Paradox Basin revisited – New developments in petroleum systems and basin analysis: Denver, Colorado* (pp. 222–264). Denver, CO: Rocky Mountain Association of Geologists, Special Publication.
- Coleman, A., Jackson, C. A.-L., Duffy, O. B., & Nikolinakou, M. A. (2018). How, where, and when do radial faults grow near salt diapirs? *Geology*, 48, 655–658. <https://doi.org/10.1130/G40338.1>
- Condon, S. M. (1997). Geology of the Pennsylvanian and Permian Cutler Group and Permian Kaibab Limestone in the Paradox Basin, southeastern Utah and southwestern Colorado. US Department of the Interior, US Geological Survey Bulletin 2000-P.
- Davison, I., Alsop, I., Birch, P., Elders, C., Evans, N., Nicholson, H., ... Young, M. (2000). Geometry and late-stage structural evolution of Central Graben salt diapirs, North Sea. *Marine and Petroleum Geology*, 17, 499–522. [https://doi.org/10.1016/S0264-8172\(99\)00068-9](https://doi.org/10.1016/S0264-8172(99)00068-9)
- Deatrick, K. T., Giles, K., Langford, R., Rowan, M. G., & Hearon, T. E. (2015). Geometry and depositional facies of an exposed megaflysch: Pennsylvanian Honaker Trail Formation, Gypsum Valley salt wall, Paradox Basin, Colorado (abstract). AAPG Annual Convention and Exhibition, Denver, CO, May 31–June 3.
- DeCelles, P. G., & Giles, K. A. (1996). Foreland basin systems. *Basin Research*, 8, 105–123. <https://doi.org/10.1046/j.1365-2117.1996.01491.x>
- Diegel, F. A., Karlo, J. F., Schuster, D. C., Shoup, R. C., & Tauvers, P. R. (1995). Cenozoic structural evolution and tectono-stratigraphic framework of the Northern Gulf Coast continental margin. In M. P. A. Jackson, D. G. Roberts & S. Snelson (Eds), *Salt tectonics a global perspective*. AAPG Memoir, 65, 109–151.
- Doelling, H. H. (1988). Geology of Salt Valley Anticline and Arches National Park, Grand County, Utah. In H. H. Doelling, C. G. Oviatt & P. W. Huntoon (Eds), *Salt deformation in the Paradox Region. Utah Geological and Mineral Survey Bulletin*, 122, 7–58.
- Doelling, H. H. (2001). Geologic map of the Moab and eastern part of the San Rafael Desert 30' x 60' Quadrangles, Grand and Emery Counties, Utah and Mesa County, Colorado. Utah Geological Survey Map 180.
- Elston, D. P., Shoemaker, E. M., & Landis, E. R. (1962). Uncompahgre front and salt anticline region of Paradox Basin, Colorado and Utah. *AAPG Bulletin*, 46, 1857–1878.
- Fleming, M. W. (2015). *Integrated structural and fracture analysis of Lisbon Valley salt anticline, Utah*. MSc. Thesis, Northern Illinois University, DeKalb, IL.
- Franczyk, K. J. (1992). Measured section of the Pennsylvanian Hermosa Group near Hermosa, Colorado (pp. 5). US Department of the Interior, US Geological Survey Open-File Report, 92-689.
- Ge, H., Jackson, M. P. A., & Vendeville, B. C. (1997). Kinematics and dynamics of salt tectonics driven by propagation. *AAPG Bulletin*, 81, 398–423.
- Giles, K. A., & Lawton, T. F. (2002). Halokinetic sequence stratigraphy adjacent to the El Papalote diapir, northeastern Mexico. *AAPG Bulletin*, 86, 823–840.
- Giles, K. A., & Rowan, M. G. (2012). Concepts in halokinetic-sequence deformation and stratigraphy. In G. I. Alsop, S. G. Archer, A. J. Hartley, N. T. Grant & R. Hodgkinson (Eds), *Salt tectonics, sediments and prospectivity. Geological Society, London, Special Publications*, 363, 7–31. <https://doi.org/10.1144/sp363.2>
- Goldhammer, R. K., Oswald, E. J., & Dunn, P. A. (1994). High-frequency, glacio-eustatic cyclicity in the Middle Pennsylvanian of the Paradox Basin – an evaluation of Milankovitch forcing. In deBoer P. L. & D. G. Smith (Eds), *Orbital forcing and cyclic sequences*. Special publication of International Association of Sedimentologists, 19, 243–283.
- Graham, R., Jackson, M., Pilcher, R., & Kilsdonk, B. (2012). Allochthonous salt in the sub-Alpine fold-thrust belt of Haute Provence, France. In G. I. Alsop, S. G. Archer, A. J. Hartley, N. T. Grant & R. Hodgkinson (Eds), *Salt tectonics, sediments and prospectivity. Geological Society, London, Special Publications*, 363, 595–615. <https://doi.org/10.1144/sp363.30>
- Harrison, J. C., & Jackson, M. P. A. (2014). Exposed evaporite diapirs and minibasins above a canopy in central Sverdrup Basin,

- Axel Heiberg Island, Arctic Canada. *Basin Research*, 26, 567–596. <https://doi.org/10.1111/bre.12037>
- Hazel, J. E. (1994). Sedimentary response to intrabasinal salt tectonism in the Upper Triassic Chinle Formation, Paradox basin, Utah. US Department of the Interior, US Geological Survey Bulletin, 2000-F, 34.
- Hearon, T. E. IV, Rowan, M. G., Giles, K. A., & Hart, W. H. (2014). Halokinetic deformation adjacent to the deep-water Auger diapir, Garden Banks 470, northern Gulf of Mexico: Testing the applicability of an outcrop-based model using subsurface data. *Interpretation*, 2, SM57–SM76. <https://doi.org/10.1190/int-2014-0053.1>
- Hite, R. J., & Buckner, D. H. (1981). Stratigraphic correlations, facies concepts, and cyclicity in Pennsylvanian rocks of the Paradox Basin. In D. L. Wiegand (Ed.), *Geology of the Paradox Basin* (pp. 147–159). Denver, CO: Rocky Mountain Association of Geologists.
- Hudec, M. R. (1995). The Onion Creek salt diapir: An exposed diapir fall structure in the Paradox basin, Utah. In C. J. Travis, H. Harrison, M. R. Hudec, B. C. Vendeville, F. J. Peel & B. E. Perkins (Eds.), *Salt, sediment and hydrocarbons* (pp. 125–134). SEPM Foundation, Gulf Coast Section, 16th Annual Research Conference Program with Papers.
- Hudec, M. R., & Jackson, M. P. A. (2011). The salt mine: A digital atlas of salt tectonics: The University of Texas at Austin, Bureau of Economic Geology, Udden Book Series No. 5. *AAPG Memoir*, 99, 305.
- Hossack, J. (1995). Geometric rules of section balancing for salt structures. In M. P. A. Jackson, D. G. Roberts & S. Snelson (Eds.), *Salt tectonics: A global perspective. American Association of Petroleum Geologists Memoir*, vol. 65, 29–40.
- Jackson, M. P. A., & Vendeville, B. C. (1994). Regional extension as a geologic trigger for diapirism. *GSA Bulletin*, 106, 57–73. [https://doi.org/10.1130/0016-7606\(1994\)106<0057:REAAGT>2.3.CO;2](https://doi.org/10.1130/0016-7606(1994)106<0057:REAAGT>2.3.CO;2)
- Kergaravat, C., Ribes, C., Legeay, E., Callot, J.-P., Kavak, K. S., & Ringenbach, J.-C. (2016). Minibasins and salt canopy in foreland fold-and-thrust belts: The central Sivas Basin, Turkey. *Tectonics*, 35, 1342–1366. <https://doi.org/10.1002/2016TC004186>
- Kluth, C. F. (1986). Plate tectonics of the Ancestral Rocky Mountains. In J. A. Peterson (Ed.), *Paleotectonics and sedimentation in the Rocky Mountain Region, United States. AAPG Memoir*, 41, 353–369.
- Kluth, C. F., & Coney, P. J. (1981). Plate tectonics of the Ancestral Rocky Mountains. *Geology*, 9, 10–15. [https://doi.org/10.1130/0091-7613\(1981\)9<10:ptotar>2.0.co;2](https://doi.org/10.1130/0091-7613(1981)9<10:ptotar>2.0.co;2)
- Kluth, C. F., & DuChene, H. R. (2009). Late Pennsylvanian and early Permian structural geology and tectonic history of the Paradox Basin and Uncompahgre uplift, Colorado and Utah. In W. S. Houston, L. L. Wray & P. G. Moreland (Eds.), *The Paradox Basin revisited—New developments in petroleum systems and basin analysis* (pp. 178–197). Denver, CO: Rocky Mountain Association of Geologists, Special Paper (CD-ROM).
- Krzywiec, P. (2006). Structural inversion of the Pomeranian and Kuiavian segments of the Mid-Polish Trough – lateral variations in timing and structural style. *Geological Quarterly*, 50, 151–168.
- Lawton, T. F., & Buck, B. J. (2006). Implications of diapir-derived detritus and gypsic paleosols in Lower Triassic strata near the Castle Valley salt wall, Paradox Basin, Utah. *Geology*, 34, 885–888. <https://doi.org/10.1130/G22574.1>
- Lawton, T. F., Buller, C. D., & Parr, T. R. (2015). Provenance of a Permian erg on the western margin of Pangea: Depositional system of the Kungurian (late Leonardian) Castle Valley and White Rim sandstones and subjacent Cutler Group, Paradox Basin, Utah, USA. *Geosphere*, 11, 1475–1506. <https://doi.org/10.1130/GES01174.1>
- Lawton, T. F., Sprinkel, D. A., Decelles, P. G., Mitra, G., Sussman, A. J., & Weiss, M. P. (1997). Stratigraphy and structure of the Sevier thrust belt and proximal foreland-basin system in central Utah: A transect from the Sevier Desert to the Wasatch Plateau. *Brigham Young University Geology Studies*, 42, 33–67.
- Mahrer, K., Ake, J., O'Connell, D., & Block, L. (2012). 2002 Status report-paradox valley seismic network. Paradox Valley Project, Southwestern Colorado, U.S. Department of the Interior, Seismotectonics and Geophysics Group. Technical Memorandum No. D8330-2003-009, Bureau of Reclamation.
- Mallory, W. W. (1972). Pennsylvanian system: Regional synthesis. In: W. W. Mallory (Ed.), *Geologic Atlas of the Rocky Mountain Region* (pp. 111–128). Denver, CO: Rocky Mountain Association of Geologists.
- Mankowski, L. C., Campbell, T. R., Huntoon, J. E., Gregg, W. J., & Linari, D. J. (2002, July 21–26). Structural mapping of the Uncompahgre front near Gateway, Colorado, with emphasis on Ancestral Rocky Mountain fabrics. AAPG Hedberg Conference, Vail, CO.
- Martín-Martín, J. D., Vergés, J., Saura, E., Moragas, M., Messenger, G., Baqués, V., ... Hunt, D. W. (2016). Diapiric growth within an Early Jurassic rift basin: The Tazoult salt wall (central High Atlas, Morocco). *Tectonics*, 35, 1–31. <https://doi.org/10.1002/2016TC004300>
- Mast, A. M. (2016). *The origin of anomalous carbonate units outcropping at the salt-sediment interface of the southern end of Gypsum Valley salt wall, Paradox Basin, Colorado*. MSc. Thesis, University of Texas at El Paso, El Paso, TX.
- McFarland, J., Giles, K. A., Langford, R., & Rowan, M. G. (2015, September 20–22). Structural and stratigraphic development of a salt diapir shoulder, Gypsum Valley Salt Wall, Paradox Basin, Colorado (abstract). Gulf Coast Association of Geological Societies Convention, Houston, TX.
- Mohr, M., Kukla, P. A., Urai, J. L., & Bresser, G. (2005). Multiphase salt tectonic evolution in NW Germany: Seismic interpretation and retro-deformation. *International Journal of Earth Sciences*, 94, 917–940. <https://doi.org/10.1007/s00531-005-0039-5>
- Molenaar, C. M. (1981). Mesozoic stratigraphy of the Paradox basin: An overview. In D. L. Wiegand (Ed.), *Geology of the Paradox basin* (pp. 119–127). Rocky Mountain Association of Geologists Field Conference.
- Moore, K. D., Soreghan, G. S., & Sweet, D. E. (2008). Stratigraphic and structural relations in the proximal Cutler Formation of the Paradox Basin: Implications for timing of movement on the Uncompahgre front. *The Mountain Geologist*, 45, 49–68.
- Morrison, S. J., & Parry, W. T. (1986). Deposits from Saline Basin Brines, Lisbon Valley, Utah. *Economic Geology*, 81, 1853–1866. <https://doi.org/10.2113/gsecongeo.81.8.1853>
- Nuccio, V. F., & Condon, M. (1996). Burial and thermal history of the Paradox basin, Utah and Colorado, and petroleum potential of the Middle Pennsylvanian Paradox Formation, US Department of the Interior. US Geological Survey Bulletin, 2000-O, 41.-->

- O'Sullivan, R. B., & MacLachlan, M. E. (1975). Triassic rocks of the Moab-White Canyon area, southeastern Utah. In Canyonlands Country: Four Corners Geological Society, Eighth Field Conference, Guidebook (pp. 129–142).
- Parker, J. M. (1981). Lisbon Field Area, San Juan County, Utah. In: D. L. Wiegand (Ed.), *Geology of the Paradox Basin field conference*, Rocky Mountain Association of Geologists, AAPG Memoir 9 Natural Gases of North America, 5, 2009.
- Pevear, D. R., Vrolijk, P. J., & Longstaffe, F. J. (1997). Timing of Moab Fault displacement and fluid movement integrated with burial history using radiogenic and stable isotopes. In J. P. Hendry (Ed.), *Geofluids II – Extended abstracts* (pp. 42–45). Belfast, UK: Geofluids Research.
- Rasmussen, L., & Rasmussen, D. L. (2009). Burial history analysis of the pennsylvanian petroleum system in the Deep Paradox Basin Fold and Fault Belt, Colorado and Utah. In: W. S. Houston, L. L. Wray & P. G. Moreland (Eds), *The Paradox Basin revisited: New developments in petroleum systems and basin analysis* (pp. 24–94). Rocky Mountain Association Geologist Special Publication.
- Rowan, M. G., Giles, K. A., Hearon, T. E. IV, & Fiduk, J. C. (2016). Megaflaps adjacent to salt diapirs. *AAPG Bulletin*, 11, 1723–1747. <https://doi.org/10.1306/05241616009>
- Rowan, M. G., & Inman, K. F. (2005). Counterregional-style deformation in the Deep Shelf of the Northern Gulf of Mexico. *Gulf Coast Association of Geological Societies Transactions*, 55, 947–969.
- Rowan, M. G., & Inman, K. F. (2011). Salt-related deformation recorded by allochthonous salt rather than growth strata. *Gulf Coast Association of Geological Societies Transactions*, 61, 379–390.
- Rowan, M. G., Jackson, M. P. A., & Trudgill, B. D. (1999). Salt-related fault families and fault welds in the northern Gulf of Mexico. *AAPG Bulletin*, 9, 1454–1484.
- Rowan, M. G., Lawton, T. F., & Giles, K. A. (2012). Anatomy of an exposed vertical salt weld and flanking strata, La Popa Basin, Mexico. In G. I. Alsop, S. G. Archer, A. J. Hartley, N. T. Grant & R. Hodgkinson (Eds), *Salt tectonics, sediments and prospectivity* (pp. 33–57). Geological Society, London, Special Publications, 363. <https://doi.org/10.1144/sp363.3>
- Rowan, M. G., Lawton, T. F., Giles, K. A., & Ratliff, R. A. (2003). Near-salt deformation in La Popa basin, Mexico, and the northern Gulf of Mexico: A general model for passive diapirism. *AAPG Bulletin*, 87, 733–756. <https://doi.org/10.1306/01150302012>
- Rowan, M. G., & Lindsø, S. (2017). Salt tectonics of the Norwegian Barents Sea and Northeast Greenland Shelf. In J. I. Soto, J. F. Flinch, & G. Tari (Eds.), *Permo-Triassic Salt Provinces of Europe, North Africa and the Atlantic Margins* (pp. 265–286). Amsterdam, the Netherlands: Elsevier.
- Saura, E., Vergés, J., Martín-Martín, J. D., Messager, G., Moragas, M., Razin, P., ... Hunt, D. W. (2013). Syn- to post-rift diapirism and minibasins of the Central High Atlas (Morocco): The changing face of a mountain belt. *Journal of the Geological Society*, 171, 97–105. <https://doi.org/10.1144/jgs2013-079>
- Schultz-Ela, D. D., Jackson, M. P. A., & Vendeville, B. C. (1993). Mechanics of active salt diapirism. *Tectonophysics*, 228, 275–312. [https://doi.org/10.1016/0040-1951\(93\)90345-K](https://doi.org/10.1016/0040-1951(93)90345-K)
- Schuster, D. C. (1995). Deformation of Allochthonous Salt and Evolution of Related Salt-structural Systems, Eastern Louisiana Gulf Coast. In M. P. A. Jackson, D. G. Roberts & S. Snelson (Eds), *Salt tectonics a global perspective*. AAPG Memoir, 65, 177–198.
- Shoemaker, E. M., Case, J. E., & Elston, D. P. (1958). Salt anticlines of the Paradox Basin. *Guidebook 9th Annual Field Conference* (pp. 39–59). Intermountain Association of Petroleum Geologists: Salt Lake City, UT.
- Solum, J. G., van der Pluijm, B. A., & Peacor, D. R. (2005). Neocrystallization, fabrics and age of clay minerals from an exposure of the Moab Fault, Utah. *Journal of Structural Geology*, 27, 1563–1576. <https://doi.org/10.1016/j.jsg.2005.05.002>
- Stewart, S. A. (2006). Implications of passive salt diapir kinematics for reservoir segmentation by radial and concentric faults. *Marine and Petroleum Geology*, 23, 843–853. <https://doi.org/10.1016/j.marpetgeo.2006.04.001>
- Stewart, S. A. (2007). Salt tectonics in the North Sea Basin: A structural style template for seismic interpreters. In A. C. Ries, R. W. H. Butler & R. H. Graham (Eds), *Deformation of the continental crust: The Legacy of Mike Coward* (pp. 361–396). Geological Society, London, Special Publications, 272.
- Stewart, J. H., Poole, F. G., & Wilson, R. F. (1972). Stratigraphy and origin of the Triassic Moenkopi Formation and related strata in the Colorado Plateau region. US Department of the Interior. *US Geological Survey Professional Paper*, 691, 195.
- Timbel, C. B. (2015). *Uncompahgre Fault Geometry: a Seismic, Field, and Gravity Study Near Nucla, Colorado, Paradox Basin, USA*. MSc. Thesis, Colorado School of Mines, Golden, CO.
- Trudgill, B. (2011). Evolution of salt structures in the northern Paradox Basin: Controls on evaporite deposition, salt wall growth and supra-salt stratigraphic architecture. *Basin Research*, 23, 208–238. <https://doi.org/10.1111/j.1365-2117.2010.00478.x>
- Trudgill, B., Banbury, N., & Underhill, J. (2004). Salt evolution as a control on structural and stratigraphic systems: Northern Paradox foreland basin, SE Utah, USA. In P. J. Post (Ed.), *Salt-Sediment Interactions and Hydrocarbon Prospectivity: Concepts, Applications and Case Studies for the 21st Century*. Gulf Coast Society of Economic Paleontologists and Mineralogists Foundation, 24th Bob F. Perkins Research Conference Proceedings (CD-ROM) (pp. 669–700). Houston, TX: Gulf Coast Section SEPM Foundation.
- Trudgill, B. D., & Paz, M. (2009). Restoration of Mountain Front and salt structures in the Northern Paradox Basin, SE Utah. In W. S. Houston, L. L. Wray & P. G. Moreland (Eds), *The Paradox Basin revisited: New developments in Petroleum systems and basin analysis* (pp. 132–177). Rocky Mountain Association of Geologist Special Publication.
- Trudgill, B. D., & Rowan, M. G. (2004). Integrating 3D seismic data with structural restorations to elucidate the evolution of a stepped counter-regional salt system, Eastern Louisiana Shelf, Northern Gulf of Mexico. In R. J. Davies, J. A. Cartwright, S. A. Stewart, M. Lappin & J. R. Underhill (Eds), *3D Seismic technology: Application to the exploration of sedimentary basins* (pp. 165–176). Geological Society, London, Memoirs 29.
- Trusheim, F. (1960). Mechanism of Salt Migration in Northern Germany. *AAPG Bulletin*, 44, 1519–1540.
- Vogel, J. D. (1960). Geology and ore deposits of the Klondike Ridge Area, CO: U.S. Geological Survey, Open-File Report USGS Numbered Series 60–145.
- Weimer, P. C. (1982). Upper Cretaceous stratigraphy and tectonic history of the Ridgway area, northwestern San Juan Mountains. *Colorado. The Mountain Geologist*, 19(4), 91–104.

- Whidden, K. J., Lillis, P. G., Anna, L. A., Pearson, K. M., & Dubiel, R. F. (2013). Geology and total petroleum systems of the Paradox Basin, Utah, Colorado, New Mexico, and Arizona. *The Mountain Geologist*, 51, 119–138.
- White, M. A., & Jacobson, M. I. (1983). Structures associated with the southwest margin of the ancestral Uncompahgre Uplift. In W. R. Averett (Ed.), *Northern Paradox Basin – Uncompahgre uplift* (pp. 33–39). Grand Junction, CO: Grand Junction Geological Society.

How to cite this article: Escosa FO, Rowan MG, Giles KA, et al. Lateral terminations of salt walls and megafaults: An example from Gypsum Valley Diapir, Paradox Basin, Colorado, USA. *Basin Res.* 2019;31:191–212. <https://doi.org/10.1111/bre.12316>